Protective Effect on Bone of Nacre Supplementation in Ovariectomized Rats

Dung Kim Nguyen, Norbert Laroche, Arnaud Vanden-Bossche, Marie-thérèse Linossier, Mireille Thomas, Sylvie Peyroche, Myriam Normand, Yacine Bertache-Djenadi, Thierry Thomas, Hubert Marotte, et al.

Title Page

Protective effect on bone of nacre supplementation in ovariectomized rats

Dung Kim NGUYEN [1], Norbert LAROCHE [1], Arnaud VANDEN-BOSSCHE [1], Marie-Thérèse LINOSSIER [1], Mireille THOMAS [1], Sylvie PEYROCHE [1], Myriam NORMAND [1], Yacine BERTACHE [1], Thierry THOMAS [1,2], Hubert MAROTTE [1,2], Laurence VICO [1], Marie-Hélène LAFAGE-PROUST [1,2], Marthe ROUSSEAU [1,3]

[1] U1059 SAINBIOSE, INSERM, Univ Jean Monnet, Univ Lyon, Mines Saint-Étienne, Saint-Étienne, France

[2] Department of Rheumatology, Hôpital Nord, CHU Saint-Etienne, Saint-Etienne, France

[3] University of Lyon, INSA-Lyon, CNRS, MATEIS (UMR 5510), Villeurbanne, France

Running title: **Nacre supplementation limits bone loss**

Corresponding author: **Marthe Rousseau**, telephone: +33477421472, e-mail: marthe.rousseau@univ-st-etienne.fr, 10 rue de la Marandière - 42270 Saint-Priest-en-Jarez, France. http://orcid.org/0000-0003-0503-5651

Table count: 4

Figure count: 6

Reference count: 48

Abstract – Word count: 279

Nacre has emerged as a beneficial natural product for bone cells and tissues, but its effect was only studied by gavage in the ovariectomized mouse model. We sought to assess the anti-osteoporotic effect of nacre through a nutritional supplementation in the ovariectomized rat model.

Sixteen-week-old female Wistar rats were either Sham-operated or bilateral ovariectomized (OVX) and then fed with a standard diet (Sham and OVX groups) or a standard diet supplemented with either 0.25% $CaCO_3$ or nacre (OVX $CaCO_3$ and OVX Nacre group, respectively) during 28 days (n=10/group). The bone microarchitecture was assessed at appendicular, and axial bones by micro-computed tomography (µCT). Histomorphometric analysis was performed to determine cellular and dynamic bone parameters. Bone metabolism was also evaluated by biochemical markers and gene expression levels.

Nacre-based diet prevented the OVX-induced bone loss better than that of $CaCO_3$ supplement, given the significant changes in trabecular bone volume fraction (BV/TV) both at the femoral distal metaphysis (difference, 35%; P=0.004) and at the second lumbar spine (difference, 11%; P=0.01). Trabecular osteoclast surfaces (Oc.S/BS) were also 1.5-fold lower at the tibial proximal metaphysis in OVX Nacre group compared to OVX $CaCO_3$ group (P=0.02). By PCA analysis, OVX Nacre group formed a cluster away from OVX group and with a trend the closest to Sham group. These data were consistent with biological measurements demonstrating a positive profile related to nacre supplementation, which blunted an increase in serum CTX level and enhanced serum P1NP secretion after 14 days post-OVX, compared to $CaCO_3$ supplementation.

We conclude that supplementation with nacre could effectively limit bone loss induced by estrogen deficiency just following OVX in rats by modulating the negative imbalance of bone turnover driving these changes.

Keywords: bone, osteoporosis, ovariectomy, rats, nacre

1. Introduction

Osteoporosis is a common and widespread skeletal disease which increases the risk of fragility fracture [1]. It is characterized by an imbalance of bone remodeling that leads to a systemic impairment of bone mass, strength, and microarchitecture. Although both men and women gradually lose bone as part of the aging process, a greater loss is observed in postmenopausal women associated with estrogen deficiency [2]. The incidence of fracture increases with age in both sexes, but age‐adjusted rates are 49% greater in females than in males [3]. In addition, following an initial fracture, women increase their risk of sustaining a second fracture by 36% [4] and from the age of 60, the residual lifetime risk of fracture is ~50% in women [5]. Thus, postmenopausal osteoporosis related to its clinical consequences, including morbidity and mortality imposes a significant health care problem for society.

Today, there is a need to develop novel approaches for osteoporosis treatment with fewer adverse effects than current therapies. It is encouraging that products of natural origin, such as plant-derived extracts [6,7], marine animal-derived products [8-10], and fungi's metabolite [11] appear to be reliable sources for the development of anti-osteoporotic agents, due to their efficacy and safety. Nacre (mother-of-pearl) has been considered one of the potential candidates.

Nacre is produced by mollusks and is composed of crystalline calcium carbonate ($CaCO_3$) embedded in an organic matrix [12]. This inorganic microstructure coupled with the organic phase contributes to the bioactivity of nacre, as a novel biomaterial [13]. Furthermore, several nacre matrix factors have been identified and known to have biological activities on bone cells. Protein PFMG1 [14] and water/ethanol-soluble matrix [15,16] have been derived from *Pinctada*'s pearl oyster family, which accelerate osteoblast differentiation. Besides the regulation of mineralization, protein N16 [17] and other molecules [18] from nacre have been demonstrated to inhibit osteoclastogenesis. These properties of nacre have directedresearchs toward its effect on osteoporosis.

The preclinical studies revealed that nacreous factors prevent induced bone loss [8,14]. Most of these studies have been conducted in ovariectomized mouse models under oral administration (gavage) or virus injection technics, whereas our experimental powders were integrated into dietary foods, which

aimed to respect the 3R principles of animal welfare, and are also considered a classic nutritional supplementation in human.

In the large variety of animal species, including rodents, non-rodents (i.e., rabbits, dogs, primates) have been used as animal models in osteoporosis research, and no single animal species duplicates all the characteristics of human osteoporosis, and each species exhibits its limitation [19,20]. Here, we performed the ovariectomy, which mimics a condition similar to menopause, and also chose the rat model, which bears a strong resemblance to human osteopenia, both in its anatomical features as well as in the transitional and steady stages of the bone dynamics [19]. Indeed, the Guideline on the Evaluation of New Medicinal Products in the Treatment of Primary Osteoporosis elaborated by the Committee for Medicinal Products for Human Use (CHMP) of the European Medicines Agency (London, 2006) recommended performing preclinical studies of bone quality in two animal species, one of which should be ovariectomized rat, and the non-rodent animal with estrogen deficiency and characterized by evaluable cortical remodeling [21].

Moreover, it is known that in osteoporotic women the first and most severe bone changes occur in the spongy bone of the vertebral body, whereas in rats they predominantly involve the trabecular bone of the metaphyseal region of the long bones [22]. Also, the bone sites display different responses to bone loss stimuli related to their structural and metabolic characteristics [6,19]. Hence, we thought that investigating the effect of nacre on both appendicular and axial bones would provide more translational insights into this novel research direction.

To test the hypothesis that dietary nacre powder may have a protective effect against bone loss in the ovariectomized rat, we pursue two specific aims: (i) to quantify the prevention of bone loss due to estrogen deficiency at several skeletal sites and (ii) to explore the nacre action mechanisms through biomarkers involved in bone metabolism.

2. Materials and Methods

2.1. Animal experimentation

Eight-week-old female Wistar rats (mean ± SD body weight: 166.8 ± 11.8 g) were housed under controlled conditions (22 °C ± 1 °C, 50-80% relative humidity; 12 hours light-dark cycle) in groups of two animals per cage with free access to water and food *ad libitum*. The animals benefited from quality attention and care by qualified personnel, both during and outside of procedures, to ensure optimal well-being throughout the study. This study was carried out with the approval of the French Ministry of Research and Innovation (approval no. APAFIS # 13401-2018020615412128 v6). Animal procedures were performed in an accredited animal facility (authorization no. 42180801) at the PLEXAN (Platform for Animal Experimentation and Analysis, Medical School, Saint-Etienne, France) with the approval of the Animal Ethics Committee and by directive 2010/63/EU and the "Principles of Laboratory Animal Care" recommended by the National Society for Biomedical Research in France. All animal handling and experimental protocols followed the ethical standards established in the 1964 Declaration. 16-week-old animals (mean ± SD body weight: 237.6 ± 14.1 g) were assigned to one of the four groups (n = 10 per group): i) Sham; ii) OVX; iii) OVX with $CaCO_3$ (OVX $CaCO_3$); iv) OVX with nacre (OVX Nacre). Rats were anesthetized with 2.5% Isoflurane and bilateral ovariectomy (OVX) was then performed via two ventrolateral incisions. The sham operation consisted in pulling the ovaries out of the abdominal cavity after skin incision, placing them back in the abdominal cavity, and suturing. No postoperative complications were observed.

Both Sham and OVX groups received a standard diet purchased by SAFE® diets (containing 8.5 mg calcium /g food) and the last two groups received the standard diet mixed with 0.25% supplemental $CaCO_3$ or nacre powder. The diet was initiated on the day of surgery and was maintained for 28 days after OVX. *Pinctada maxima*'s nacre powder provided by Stansea, which is composed of 97% $CaCO_3$ (i.e. 38% Calcium) was compared to aragonite $CaCO_3$ (i.e. 40% Calcium) synthesized according to the protocol of Carteret et al [23]. Calcium content was the same for both the $CaCO_3$ and nacre diets and 12% higher than the standard diet. The composition of the diets is shown in Tab. S1.

At the end of the study, rats were injected intraperitoneally with tetracycline (25 mg/kg body weight) on day 12 and 3 before killing to allow the bone histodynamic evaluation. Animals were weighed on arrival, before OVX and every two weeks during the study. All animals were killed at the age of 20 weeks using isoflurane (4%) and cardiac puncture. The uterus was dissected and immediately weighed to check OVX efficacy.

2.2. **Bone microarchitectural analysis**

We performed *in vivo* μCT longitudinal analysis of the proximal tibia including trabecular and cortical bone on the same acquisition by MicroCT40 (Scanco). The scanning system was calibrated at 70kVp, 110μA, and 1000 projections by 180 degrees with an integration time of 250 ms at high resolution (isotropic voxel size at 15μm^3 Field of View (FOV) / diameter 30.7mm). Rats were anesthetized and maintained on anesthetic Isoflurane 2% for the duration of each measurement (approximately 25 min per rat). Tibiae were scanned from the proximal growth plate and processed distally for 421 slices (6.32 mm) (Fig. 1A). CT Analyzer V6.6 software was used for measuring bone volume.

During the dissection, right tibiae, right femora, and second lumbar spines were harvested and immediately fixed for 72h in 10% neutral-buffered formalin and stored in 70% ethanol solution at 4°C. These bones were scanned by the same μCT system at 10.5μm^3 FOV / diameter of 21.5mm. A detailed description of scanning and evaluation procedures is provided in Supplemental Materials (Section 1 and Tab. S2).

2.3. **Bone Histomorphometry**

A description of the methods is provided in Supplemental Materials (Section 2).

2.4. **RNA isolation and quantitative RT-PCR analysis**

The bone marrow and the cortical fraction of the left femur were separated by flushing with a syringe and then immediately frozen in liquid nitrogen. Total RNA was extracted by TRI Reagent® (Sigma, St Louis, MO) and then purified with a Qiagen pure tissue kit (RNeasy Plus Mini Kit, Qiagen, Valencia, CA). The RNA quality was assessed by Experion automated electrophoresis station (BioRad, Hercules, CA), followed by Ribogreen assay (Quant-iT RiboGreen RNA assay kit, Invitrogen, Life

Technologies, Eugene, OR) for accurate RNA quantification. Total RNA reverse transcription was performed with an iScript cDNA synthesis kit (BioRad). Quantitative real-time (qRT) polymerase chain reaction (PCR) was conducted on CFX96 RealTime System (BioRad) with LightCycler FastStart DNA Master plus SYBRgreen I (Roche Diagnostics, Basel, Switzerland). The mRNA expression levels were normalized to the house-keeping *Hprt1* gene expression using the ΔCt method [24]. Primer sequences are shown in Tab. S3.

2.5. **Biochemical markers in blood**

Rats were fasted overnight before each blood collection by intravenous puncture in the tail on surgery day (D0: start point) and day 14 (D14: intermediate point), and by cardiac puncture under anesthesia at the end of the study (D28: endpoint). Blood was centrifuged at 13000g for 2 min at room temperature for D0 and D14 samples or 2000g for 10 min at 4°C for D28 samples and separated in serum and plasma, then stored at -80°C. Serum levels of C-terminal collagen cross-linking telopeptide of type I collagen (CTX), procollagen type I N-terminal propeptide (P1NP) and osteocalcin (Osteocalcin) were quantified by ELISA commercial kits according to manufacturer protocols (Ratlaps CTX-I EIA kits, Rat/Mouse P1NP EIA kits and Rat-MID Osteocalcin EIA, Immunodiagnostic Systems, Paris, France, respectively). Serum calcium and inorganic phosphate levels were measured with colorimetric assays (Kit Biolabo SAS, Maizy, France). In addition, levels of parathyroid hormone (PTH) and fibroblast growth factor 23 (FGF23) in plasma were measured by Rat Intact PTH ELISA kit (Immunotopics, San Clemente, CA) and Mouse/Rat FGF23 Intact ELISA kit (Immunotopics, San Clemente, CA), respectively.

2.6. **Statistical analyses**

Graphical data are presented as box plots, with the central box spanning 25^{th}-75^{th} percentiles and the central line representing the median. Whiskers represent the 10^{th} and 90^{th} percentiles and dots represent the sampling distribution. Graphs depicting body weight changes and serum/plasma biomarker levels are presented as line plots, with vertical bars depicting the mean and standard error (SE). Data were checked for normality and distribution using Quantile-Quantile plots and the Shapiro-

Wilk test. Numerical tabular data are shown as the median and interquartile range (IQR) or mean and standard deviation (SD). Power analysis and calculation of sample size were performed before the initiation of the study by G*Power to define the alpha level of 0.05 and the beta level of 0.15, thereby the sample size was n=10/group.

For longitudinal data analysis, (i) comparisons between groups in μCT *in vivo* study at follow-up were based on analysis of covariance (ANCOVA) general linear models using values at baseline as covariable, as a standard method [25]. Tukey's Honest Significant Difference (HSD) posthoc test was then performed to report 95% confidence intervals (CI); (ii) Biochemical marker levels in serum/plasma were analyzed by two-way repeated-measures ANOVA to determine if there were group effect (between-subjects factor), time effect (within-subjects factor), and interaction between them. After ANOVA, Tukey's HSD post-hoc test was used for multiple comparisons between groups and between the value at the time point versus that at a previous time point in each group [26].

For cross-sectional data analysis, parameters of the μCT *ex vivo* bone microarchitecture, histomorphometry, and relative gene expressions were compared between groups using ANOVA, followed by Tukey's HSD post hoc test. If the normal condition was not satisfied, the Kruskal-Wallis test was used instead, and Mann-Whitney-Wilcoxon (MWW) unpaired test was corrected by the false discovery rate adjustment method of Benjamini and Hochberg [27] was then performed for pairwise comparisons.

A nominal P-value of 0.05 was considered "statistical significance". Data analysis was conducted with R Statistical Environment and data visualization using the "ggplot2" package.

The μCT and histomorphometric *ex vivo* variables in the tibia were processed with Principal Component Analysis (PCA), an unsupervised method of Machine Learning [28], by function "prcomp" in the base R environment, and the autoscale function was applied to the dataset. Graphical visualization was shown using package "factoextra".

3. Results

3.1. Validation of the ovariectomy-induced bone loss model in rat

All rats showed a gradual increase in body weight over the first 8 weeks before OVX, according to physiological growth (Fig. S1A). Beginning from 14 days post-OVX, a weight difference of approximately 12% was observed between OVX and Sham groups (254.85 ± 8.75 versus [vs] 228.6 ± 9.82 g, $P < 0.001$). The final body weights of the OVX and Sham groups on day 28 were 271.27 ± 2.25 g and 237.25 ± 9.6 g ($P < 0.001$), respectively. The uterus weight of OVX rats was significantly lower than that of Sham ($P < 0.001$) due to estrogen deficiency-induced uterine atrophy. No significant difference in uterine weight between the different OVX groups was observed (data not shown).

The trabecular microarchitectural parameters were significantly deteriorated in OVX compared to Sham, regardless of the bone sites (Fig. 1, 2 and Tab. 2). In the tibia, after accounting for baseline, trabecular BV/TV was 55% lower (18.5 vs 41.3; 95% CI, -29.1 to -13.1, $P < 0.001$), Tb.Th was 22% lower (0.07 vs 0.09; 95% CI, -0.02 to -0.01; $P < 0.001$) and Tb.Sp was +67% higher (0.25 vs 0.15; 95% CI, 0.03 to 0.16; $P = 0.003$) in OVX group (Fig. 1B and C, Tab. 1). As expected, these quantitative parameters were similarly affected in the cross-sectional analyses (Fig. S2).

In the femur (Fig. 2 and S3), trabecular BV/TV was 43% lower ($P = 0.002$), Tb.N was 26% lower ($P < 0.001$), Tb.Th was 11% lower ($P = 0.01$) and Tb.Sp was +53% higher ($P < 0.001$) in OVX group, compared to Sham. In the second lumbar spine (Tab. 2), BV/TV and Tb.N were significantly lower in OVX group than in Sham (-12%, $P = 0.05$; and -6%, $P = 0.01$, respectively), with no change in Tb.Th. ($P > 0.10$).

We also assessed the cortical bone microarchitecture in the diaphysis of both the tibia and femur, but no change was roughly observed at day 28 post-OVX (Tab. S4).

Representative images and parameters for histomorphometry evaluation in longitudinal sections of non - decalcified tibiae are shown in Fig. 3A-D and Tab. 4. As expected, OVX induced a significant increase in bone remodeling with a 3.4-fold increase in osteoclast surface and a 3-fold increase in Bone Formation Rate ($P < 0.001$) compared to Sham.

The global visualization among the μCT and histomorphometry variables in the tibia and the rats was explored with Principal Component Analysis (PCA) (Fig. 4). The score plot shows two separate clusters that were formed by Sham group (in black) and OVX group (in red) along with the first component. This component explained up to 74.1% variance of all variables. The first loading vector places most of its weight on Tb.Sp, SMI, BFR/BS, and Oc.S/BS and much less weight on the other four features. Hence, this first component roughly corresponds to the level of trabecular quantification and bone remodeling activity of the rats.

In line with the μCT and histomorphometry results, estrogen deficiency also induced an increase in mRNA expression of gene markers involved in both osteoblastogenesis and osteoclastogenesis. As shown in Fig. 5, OVX rats exhibited the higher amounts of *Bgalp* (3-fold, $P < 0.001$) and *Runx2* mRNA (+1.70-fold, 2.37 vs 1.39; 95% CI, 0.20 to 1.76; $P = 0.009$), and both approximately 2-fold higher *NFATc1* (2.08 vs 1.16; 95% CI, 0.35 to 1.49; $P < 0.001$) and *Rank* ($P < 0.001$), compared to Sham group.

In agreement with the above results, the serum levels of bone turnover biomarkers were significantly elevated in OVX rats concerning time (Fig. 6). There were sustained increases in osteocalcin and CTX levels over time, whereas PINP levels showed a transient increase on day 14 and resumed baseline values thereafter. Sham rats gradually declined the secretion of these markers over time (Fig. 6).

3.2. Effect of nacre against weight gain and bone loss in comparison to standard and $CaCO_3$ diet in OVX rats

Body weight. Because of the significant differences in body weight between groups observed at the beginning of the study ($P = 0.04$) (Fig. S1A), we transformed the raw data set into symmetric percent change from baseline values before conducting pairwise comparisons between OVX groups (Fig. S1B). From baseline, nacre diet significantly limited body weight gain by 44% (6.5 vs 11.6; 95% CI, -8.1 to -2.1; $P < 0.001$) and 38% (6.1 vs 10.5; 95% CI, -7.0 to -0.92; $P = 0.006$) compared with

OVX and OVX $CaCO_3$ group, respectively at day 14. Both $CaCO_3$ and nacre diets reduced by 22% of weight at the end of the study (P = 0.02).

Bone microarchitecture analysis. In the *in vivo* longitudinal survey of tibia metaphysis, bone volume BV/TV was lower 16% for the OVX group (-2.9; 95% CI, -11.0 to 4.93; P >0.10), and 20% (-3.6; 95% CI, -11.7 to 4.2; P >0.10) for OVX $CaCO_3$ group compared to OVX Nacre group in a large effect size (η_g^2 >0.40), with mean percent change from baseline in BV/TV of -55% (OVX), -56% (OVX $CaCO_3$), -48% (OVX Nacre). Supplementing with nacre also led to higher Conn.D, Tb.N, Tb.Th and to lower Tb.Sp compared to those of both standard and $CaCO_3$ diets, after accounting for baseline values (Tab. 1 and Fig. 1). Also, e*x vivo* cross-sectional evaluation performed at a higher resolution showed a similar significant positive effect of nacre on bone mass and microarchitecture (Fig. S2), while the $CaCO_3$ diet did not show any protective impact on quantitative trabecular parameters in the tibia.

In the femur distal metaphysis (Fig. 2 and S3), trabecular bone mass and microarchitecture parameters of OVX $CaCO_3$ were not different from those of the OVX group. In contrast, the nacre diet prevented trabecular BV/TV loss by about 40% compared to standard (P = 0.04) and $CaCO_3$ (P = 0.004) diets in OVX rats, as well as other microarchitectural parameters.

The OVX-induced deterioration of microarchitecture in the second lumbar spine was also moderately prevented by the nacre diet (Tab. 2). In nacre-fed OVX rats, the bone volume was significantly higher compared to standard (+8%, P = 0.04) and $CaCO_3$ (+11%, P = 0.01) diets and trabecular number and separation were equal to standard, but better than $CaCO_3$ diet (P = 0.03 and 0.02, respectively). The protective effects of nacre in the trabecular bone at various bone sites are summarized in Tab. 3 by comparing with standard and $CaCO_3$ diets in OVX rats.

Bone histomorphometry evaluation. In pairwise comparisons between the three OVX groups (Fig. 3 and Tab. 4), the osteoclast surface was significantly decreased in both OVX $CaCO_3$ (-2-fold, 1.06 vs. 2.11, P < 0.001) and OVX Nacre (-3-fold, 0.71 vs. 2.11, P < 0.001), compared to that of OVX group. Interestingly, this decrease was 1.50-fold greater in the nacre than in the $CaCO_3$ diet (P = 0.03).

Bone formation parameters in OVX $CaCO_3$ and Nacre groups remained as increased as in the OVX group, compared to Sham.

As illustrated in Fig. 4, PCA analysis showed that the OVX rats under the $CaCO_3$ diet exhibited similar features to those under standard diet, while most of the OVX rats under nacre diet had close to zero score for the first component. On the other hand, OVX Nacre rats tended to exhibit Sham's trabecular characteristics and were apart from OVX rats.

Analysis of gene expression levels. To investigate the potential molecular mechanisms underlying the effect of experimental diets ($CaCO_3$ and nacre) in OVX rats on osteoblastogenesis, we examined various signaling factors involved in osteoblast differentiation or reflecting its activity. Despite a global decrease in expression of the bone formation-related genes such as *Col1a1, Bglap,* and *Runx2* in OVX $CaCO_3$ and nacre groups compared to OVX, the mRNA amounts of these genes were more expressed in nacre than in $CaCO_3$ (Fig. 5A). By contrast, *Bmp2* mRNA levels were up-regulated by 1.30-fold in $CaCO_3$ (P = 0.05) and by 1.70-fold in nacre diet (P = 0.004) compared to standard diet in OVX rats.

Unexpectedly, while $CaCO_3$ reduced the mRNA expression of almost of osteoclastogenesis-related genes compared to standard diet in OVX rats, nacre supplementation significantly upregulated that of *Spp1* by 2.20-fold, (P = 0.01), and *Acp5* by 1.45-fold (P = 0.04) compared to the $CaCO_3$ diet, even more than also standard diet in some genes, *Cathepsin K* (+1.25-fold; 3.53 vs 2.82; 95% CI, -0.53 to 1.95; P >0.10) and *Spp1* (+1.45-fold, P = 0.05) (Fig. 5B).

Bone turnover biomarker measurements. About changes in blood biomarkers over time, the between-groups test indicated that the variable group was significant, consequently in the graph we see that the lines for four groups are rather far apart. The within-subjects test indicated that there was a significant time effect, in the other words, each group did change over time. Moreover, the interaction of time and group was significant, which means that the groups were changing over time but were changing in different ways (Fig. 6).

On day 14, $CaCO_3$ and nacre limited the OVX-induced increase in both serum osteocalcin and CTX levels. Interestingly, P1NP levels increased more under nacre (+4-fold, P = 0.02) than under $CaCO_3$ diet (+2.30-fold, P = 0.004), compared to baseline. Osteocalcin levels from baseline were similarly increased in nacre (+2.10-fold, P = 0.001) and $CaCO_3$ (+1.50-fold; P = 0.03). On day 28, $CaCO_3$ diet diminished the fluctuation of three markers related to OVX (P<0.05 or less, compared to day 14), but still more elevated than those of Sham (P < 0.05). In contrast, nacre showed a more abundance of osteocalcin and CTX than $CaCO_3$ (P = 0.02) and illustrated by approximately +1.50-fold or more versus baseline values.

We next examined whether nacre might potentially affect the calcium – phosphate homeostasis regulated by the estrogen – PTH – FGF23 axis. As shown in Fig. S5, circulating PTH change from baseline was not different at day 14 in both OVX and OVX Nacre groups and then dramatically went up to 3.6-fold higher in the OVX group at day 28 (P = 0.05), whereas that of nacre was not detected.

Nacre supplements also had a small but significant effect on serum phosphate, with a transient about 1.50-fold increase from baseline on day 14 and 28 (P = 0.02), which were not associated with significant changes in serum FGF23 levels.

4. Discussion

The products of natural origin could play a role in novel preventative strategies against osteoporosis considered a major health problem for postmenopausal women in the community [6,9,10]. The properties of nacre and its matrix factors on bone cells were examined in *in vitro* studies [15,17,18]. Published *in vivo* works also indicated the beneficial effects of nacreous factors derived from pearl oyster *Pinctada fucata* [14] and *Pteria martensii* [8] in OVX mice. Here, we provide the additional evidence for nacre powder from *Pinctada maxima* species in the osteoporotic rat model, as an appropriate preclinical model for postmenopausal bone loss.

4.1. Bone morphology and bone turnover changes related to ovariectomy in brief

Bone microarchitecture. It is recognized that the bone growth has slowed considerably, but not stopped in the mature rat model [19]. However, this accelerated bone growth is only transient and the

final observed trabecular parameters of OVX rats were lower than those of Sham rats where true bone loss occurred (Fig. 1 right column). In the other words, the negative influence of estrogen deficiency on bone balance is so dominant in the mature rat model, that ovariectomy causes a marked depletion of trabecular bone in the appendicular skeleton despite any residual growth.

The structure model index (SMI) parameter in μCT evaluation has been widely used as an indicator of the structure of trabeculae. SMI will be 0 for parallel plates, and 3 for cylindrical rods [29]. However, our μCT findings presented both negative and positive values, particularly for Sham group in the tibial (Fig. S2), femoral metaphysis (Fig. S3), and all groups in the lumbar spine (Tab. 2). The previous work mentioned that the bone surface processes both convex and concave regions, which have been measured by positive and negative SMI, respectively. The final SMI value is the sum of all components [30]. Also, this study demonstrated the negative strong correlation between BV/TV and SMI in the rat model. This suggestion should aid to explain why the bone loss in OVX groups is linked to the plate-to-rod transition of trabeculae, which results in the positive SMI in some bone sites responding to OVX after 28 days.

As expected, we found that ovariectomy in rats caused an initial rapid phase of trabecular bone loss and deterioration of bone microstructure in the metaphysis of both proximal tibia (Tab. 1, Fig. 1 and Fig. S2) and distal femur (Fig. 2 and S3), while the cortical bone was not yet affected after 28 days post-OVX, as reported in previous studies [19,31,32].

Bone histomorphology. We performed the histomorphometry analysis in the proximal tibia by Goldner's trichrome and TRAcP staining (Tab. 4). We found that the ovariectomy increased osteoclast surface and number, also an augmented bone formation rate, as demonstrated in previous results [33-35]. These findings confirmed that the increment of bone turnover occurred in the early period after estrogen depletion.

Bone turnover markers. Concerning the gene markers of the bone turnover process, Choi and colleagues reported that the relative mRNA expression levels of osteoblast-specific genes were decreased and those of osteoclast was increased in estrogen-deficient rats after 12 weeks post-OVX [33]. By contrast, another study indicated the elevation of all analyzed gene expressions after 10 weeks

[36]. The findings from the second study are consistent with our outcomes (Fig. 5), whereby both bone formation and resorption process are considerably activated caused by the ovarian function loss in our rats suffered 28 days post-OVX.

Concerning the serum markers of bone homeostasis, osteocalcin is the bone turnover marker, P1NP is a more sensitive biomarker of bone formation in osteoporosis, while CTX is a specific and sensitive biomarker of bone resorption [37]. Ovariectomy significantly increased the level of these markers, reaching a peak after 14 days. In particular, P1NP had the highest change at day 14 and declined thereafter, despite still elevation. Otherwise, osteocalcin and CTX were continuously elevated (Fig. 6 and S5A). This is correlated to the gene expression analysis that reflects the cellular activities on day 28. Our outcomes support the argument that osteopenia is detected in OVX rats as soon as 14 days post-OVX and became progressively more pronounced up to 100 days [35]. We additionally suggest that bone formation could be maximized in the initial rapid phase at day 14, then declined at later times post-OVX, while bone resorption would be sustained for a longer time, o that the increase in bone resorption exceeds the increase in bone formation.

4.2. Beneficial effects of nacre in stimulated bone loss and bone turnover context

Limitation of body weight gain due to loss of ovarian function as early as 14 days. Although both $CaCO_3$ and nacre diets limited body weight gain after 28 days post-OVX, this positive impact was detected as early as 14 days with nacre, while that of $CaCO_3$ was not (Fig. S1). Wronski et al. suggested an only partial protective effect of obesity against bone loss due to ovarian hormone deficiency and osteopenia develops regardless of body weight [38]. Moreover, the relationships between calcium intake and body weight are still obscure. Indeed, low calcium intake is associated with higher body weight in women [39]. By contrast, the interventional trials of calcium supplementation failed to show any effect on body weight and body fat [40]. Thus, the effect against weight gain of nacre should be account to its organic matrix content, which is measured at 2.7 wt% in *Pinctada maxima* nacre [41]. Because the mechanism of body weight gain compensated for bone loss associated with OVX in rats

is still unclear, the diminished body weight of nacre should be considered as a factor or a consequence explained to its protective bone effect, which is discussed below.

Protective effect of nacre on the altered trabecular morphology 28 days after OVX. In appendicular bones (tibia and femur) and lumbar spine, nacre diet partially preserved trabecular bone mass and microarchitecture parameters (Fig. 1 and 2 and Tab. 2), whereas $CaCO_3$ did not limit this deterioration at these bone sites on day 28. A study by Gala and colleagues reported that a fifteen-week-old ovariectomized rat supplemented with calcium at doses 15 and 6.6 g/kg food during 13 and 28 weeks produced an increase in femur BMD but any significant differences were detected in both young and old animals, and those were not on lumbar spine BMD [42]. Here, we used only 12% higher calcium in $CaCO_3$ and nacre diets for 4 weeks. Thus, these recognized preventive impacts in bone sites suggest that the nacre effect could be the result not only of calcium carbonate but also of organic compounds (e.g. proteins [14,17], lipid [43], water-soluble matrix [15,18], ethanol-soluble matrix [16]) which are known for their bioactive properties (e.g. acceleration of osteoblastogenesis and inhibition of osteoclastogenesis) and also meaningfully participate in the physio-pathological condition in OVX rat model.

In addition, the nacre diet significantly reduced the surface of osteoclasts better than the $CaCO_3$ diet (Tab. 4). Therefore, our results of bone morphology and cellular histomorphometry suggested that the better and earlier protective effect on the bone structure under a nacre diet was associated with a greater decrease in the number of osteoclasts compared to $CaCO_3$, while no significant differences in bone formation rate were observed between these two experimental diets at day 28. Nevertheless, the dynamic parameters derived from double-labeling histomorphometry reflect only the bone formation rate between day 12 and day 3 before dissection, not generalizing the bone remodeling situation during 28 days post ovariectomy. Thus, we need to explore the changes in bone turnover markers over time discussed below. In general, this observed effect of nacre on bone morphology could be due to an improved intestinal calcium absorption of nacre, which would result in lower severity of secondary hyperparathyroidism observed at the latest time point in the OVX group. Unless it was shown that

calcium carbonate intestinal absorption is poorer than that of another organic calcium source [44]. Thus, this explanation reinforces the beneficial effect derived from the organic matrix of nacre. In this regard, nacre inhibits the negative bone remodeling balance better than $CaCO_3$ 28 days post-OVX in rats.

Modification of elevated bone turnover in a different way from that of $CaCO_3$. We found that nacre diet enhanced the mRNA expression of genes involved in both osteoblastogenesis and osteoclastogenesis. Previous *in vitro* studies indicated that nacreous organic matrix-induced osteoblast differentiation [16] and suppressed osteoclast activity [18]. However, the present study was realized in the OVX rat model and the gene expression levels were only analyzed on femur samples on day 28. Indeed, the findings in this part should be interpreted in the context of a longitudinal study. In other words, thanks to repeated biomarker measurements at three-time points, each animal acts as its control and shows its change concerning time.

Regarding the bone turnover markers, the responses of $CaCO_3$ and nacre diets to ovarian function loss were different. $CaCO_3$ attenuated the stimulated bone turnover process in both bone formation and resorption, whereas nacre regulated the imbalanced bone homeostasis, in favor of elevating bone formation and slowing bone resorption at the initial rapid stage of 14 days and tend to moderately maintain the increased bone turnover, at least up to 28 days in this study, before transferring to the steady-state remodeling in ovariectomy intervention. Bone turnover markers are referred to as formation and resorption markers under the assumption that these are surrogates of the cellular events. Indeed, our biomarkers–related findings could explain why the gene markers of osteoblastogenesis and osteoclastogenesis were expressed more abundantly in nacre than in the $CaCO_3$ diet at day 28. Overall, nacre may have provided an additional stimulus for bone formation, that compensates bone resorption, matching with lower bone resorption after 14 days post-OVX, which lead to more protection against bone loss.

Previous studies have described that calcium level depends on the progression and severity of deficient estrogen situation and is regulated by several factors, including PTH [45]. One of the major outcomes of this study is that the estrogen deficiency leads to a fluctuated plasma PTH level at the

second time, day 14 to 28 post-ovariectomy. Nacre supplementation is capable to maintain the stability of the PTH level (Fig. S5). Additionally, FGF23 is known as a bone-derived phosphaturic hormone, synthesized by osteoblasts, and osteocytes, that acts directly on the parathyroid glands through the MAPK pathway to decrease serum PTH [46]. It has been also suggested that the indirect effect of estrogen on PTH may require the participation of FGF23 [47]. Despite no marked changes in FGF23 levels in our study on this basis, we can hypothesize, in a restriction to the relation between bone metabolism and PTH, that nacre could impact this function through activating osteoblasts.

Our study has several strengths. First, instead of using the gavage [7,8] or injection [10,11] method used in previous studies, we gave priority to preparing the diets supplemented with $CaCO_3$ or nacre to close to the 3R principles of animal welfare. Additionally, we addressed the responses to bone loss of different skeletal sites including appendicular, and axial bones, which have significant translational relevance. Also, by combining both longitudinal and cross-sectional study designs, we generated an overall interpretation for estrogen-deficient – induced bone loss in rats and thus tried to explain how nacre could protect the bone structure in live animals.

Our study also has limitations. The rat skeleton should be exposed to a pharmaceutical agent for a duration either equivalent to bone turnover rates in humans (100-200 days) and rats (40 days) [48], or at least 6 remodeling cycles to allow relevant inference on long-term bone efficacy and safety in humans [21]. Although the rat has been recommended to use as a rodent postmenopausal model, it shows a potential drawback, that is the lack of Haversian remodeling in the intra-cortical bone [20]. Lastly, the lack of control for dietary intake of the animals induced the inability to calculation about the average exposure of kg body weight to experimental powders.

5. Conclusion

In this study, we found that supplementation with nacre could effectively limit bone loss induced by estrogen deficiency following ovariectomy in rats better than $CaCO_3$. This occurred by modulating the negative imbalance of bone turnover that led to these changes. This effect might be driven by the limitation of secondary hyperparathyroidism. However, we cannot rule out an additional uncoupling

effect of nacre on bone remodeling at day 14, that could slightly stimulate bone formation. Further preclinical studies based on longer-term evaluation and the non-rodent model are still needed to confirm the efficacy and safety of nacre. It remains to identify the precise mechanisms whereby the nacreous organic matrix acts on bone.

Disclosures

Dr. Rousseau is a member of the scientific advisory board for Megabiopharma. Dr. Thomas reports receiving lecture fees from Amgen, Arrow, Biogen, BMS, Chugai, Galapagos, Grunenthal, Jansen, LCA, Lilly, MSD, Nordic, Novartis, Pfizer, Sanofi, Thuasne, Theramex, and UCB, research grants or investigators fees from Bone Therapeutics, UC.

Acknowledgments

We gratefully thank Dr Luc Malaval, U1059 INSERM – SAINBIOSE (Saint-Etienne), for contributing to the present work with critical comments on the manuscript. We also thank staffs of PLEXAN for the supervision of animal care and Stansea for providing nacre powder for nutritional supplementation. We acknowledge the financial support by the AAP UJM 2018 and by PAR AURA NUTRINACRE. DKN is supported by the project NADO (ANR18 - CE18 – 0003 - 01) of the Agence Nationale de la Recherche.

Authors' roles:

Study concept and design: MR, AVB, and LV. *In vivo* studies: MR, AVB, and NL. Micro-CT analysis: DKN, NL, and YB. Bone histomorphometry: DKN, NL, and MHLP. Blood biomarker measurements: DKN, MTL, and SP. Gene expression analysis: DKN, MTL, and MT. Data analysis: DKN and MN. Data interpretation: DKN, MHLP, and MR. Data visualization and Writing – Original and Daft Preparation: DKN. Writing – Review & Editing: DKN, MHLP, and MR. Approving final version of manuscript: DKN, MHLP, TT, HM, LV, MR.

References

1. Rachner TD, Khosla S, Hofbauer LC. Osteoporosis: now and the future. The Lancet. 2011;377(9773):1276-87.

2. Parfitt A. Bone remodeling and bone loss: understanding the pathophysiology of osteoporosis. Clinical obstetrics and gynecology. 1987;30(4):789-811.
3. Amin S, Achenbach SJ, Atkinson EJ, Khosla S, Melton III LJ. Trends in fracture incidence: a population-based study over 20 years. Journal of Bone and Mineral Research. 2014;29(3):581-9.
4. Ho-Le TP, Tran TS, Bliuc D, Pham HM, Frost SA, Center JR, et al. Epidemiological transition to mortality and refracture following an initial fracture. Elife. 2021;10:e61142.
5. Nguyen ND, Ahlborg HG, Center JR, Eisman JA, Nguyen TV. Residual lifetime risk of fractures in women and men. Journal of Bone and Mineral Research. 2007;22(6):781-8.
6. Keiler AM, Helle J, Bader MI, Ehrhardt T, Nestler K, Kretzschmar G, et al. A standardized Humulus lupulus (L.) ethanol extract partially prevents ovariectomy-induced bone loss in the rat without induction of adverse effects in the uterus. Phytomedicine. 2017;34:50-8.
7. Xu H, Yin D, Liu T, Chen F, Chen Y, Wang X, et al. Tea polysaccharide inhibits RANKL-induced osteoclastogenesis in raw264. 7 cells and ameliorates ovariectomy-induced osteoporosis in rats. Biomedicine & Pharmacotherapy. 2018;102:539-48.
8. Kim H, Lee K, Ko C-Y, Kim H-S, Shin H-I, Kim T, et al. The role of nacreous factors in preventing osteoporotic bone loss through both osteoblast activation and osteoclast inactivation. Biomaterials. 2012;33(30):7489-96.
9. Khalil WKB, Booles HF, Hafiz NAE-M, El-Bassyouni GE-T. Ameliorative effects of Brachidontes variabilis calcium carbonate against bone loss in ovariectomized rats. International Journal of Pharmacology. 2018;14(4):477-87.
10. Wang Q, Chen D, Jin H, Ye Z, Wang C, Chen K, et al. Hymenialdisine: a marine natural product that acts on both osteoblasts and osteoclasts and prevents estrogen-dependent bone loss in mice. Journal of Bone and Mineral Research. 2020;35(8):1582-96.
11. Chen K, Qiu P, Yuan Y, Zheng L, He J, Wang C, et al. Pseurotin A inhibits osteoclastogenesis and prevents ovariectomized-induced bone loss by suppressing reactive oxygen species. Theranostics. 2019;9(6):1634.
12. Rousseau M, Lopez E, Stempflé P, Brendlé M, Franke L, Guette A, et al. Multiscale structure of sheet nacre. Biomaterials. 2005;26(31):6254-62.
13. Gerhard EM, Wang W, Li C, Guo J, Ozbolat IT, Rahn KM, et al. Design strategies and applications of nacre-based biomaterials. Acta biomaterialia. 2017;54:21-34.
14. Li L, Wang P, Hu K, Wang X, Cai W, Ai C, et al. PFMG1 promotes osteoblast differentiation and prevents osteoporotic bone loss. The FASEB Journal. 2017;32(2):838-49.
15. Chaturvedi R, Singha PK, Dey S. Water soluble bioactives of nacre mediate antioxidant activity and osteoblast differentiation. PLoS One. 2013;8(12):e84584.
16. Brion A, Zhang G, Dossot M, Moby V, Dumas D, Hupont S, et al. Nacre extract restores the mineralization capacity of subchondral osteoarthritis osteoblasts. Journal of structural biology. 2015;192(3):500-9.
17. Lin J-B, Wu H, Liu Y-L, Shaw P-C, Li P-B. N16 suppresses RANKL-mediated osteoclatogenesis by down-regulating RANK expression. International journal of biological macromolecules. 2020;151:1154-62.
18. Duplat D, Gallet M, Berland S, Marie A, Dubost L, Rousseau M, et al. The effect of molecules in mother-of-pearl on the decrease in bone resorption through the inhibition of osteoclast cathepsin K. Biomaterials. 2007;28(32):4769-78.
19. Lelovas PP, Xanthos TT, Thoma SE, Lyritis GP, Dontas IA. The laboratory rat as an animal model for osteoporosis research. Comparative medicine. 2008;58(5):424-30.
20. Turner RT, Maran A, Lotinun S, Hefferan T, Evans GL, Zhang M, et al. Animal models for osteoporosis. Reviews in endocrine & metabolic disorders. 2001;2(1):117.
21. Use CfMPfH. Guideline on the evaluation of medicinal products in the treatment of primary osteoporosis. CHMP, London. 2006;526:525-6.
22. Bonucci E, Ballanti P. Osteoporosis—bone remodeling and animal models. Toxicologic pathology. 2014;42(6):957-69.
23. Carteret C, Dandeu A, Moussaoui S, Muhr H, Humbert B, Plasari E. Polymorphism studied by lattice phonon Raman spectroscopy and statistical mixture analysis method. Application to calcium carbonate polymorphs during batch crystallization. Crystal Growth and Design. 2009;9(2):807-12.

24. Livak KJ, Schmittgen TD. Analysis of relative gene expression data using real-time quantitative PCR and the 2− ΔΔCT method. methods. 2001;25(4):402-8.
25. Vickers AJ. The use of percentage change from baseline as an outcome in a controlled trial is statistically inefficient: a simulation study. BMC medical research methodology. 2001;1(1):1-4.
26. Garcia-Valencia O, Garovic VD, Milic NM, Winham SJ. Why we need to report more than'Data were Analyzed by t-tests or ANOVA'. eLife. 2018;7.
27. Benjamini Y, Hochberg Y. Controlling the false discovery rate: a practical and powerful approach to multiple testing. Journal of the Royal statistical society: series B (Methodological). 1995;57(1):289-300.
28. James G, Witten D, Hastie T, Tibshirani R. An introduction to statistical learning: Springer; 2013.
29. Hildebrand T, Rüegsegger P. Quantification of bone microarchitecture with the structure model index. Computer Methods in Biomechanics and Bio Medical Engineering. 1997;1(1):15-23.
30. Salmon PL, Ohlsson C, Shefelbine SJ, Doube M. Structure model index does not measure rods and plates in trabecular bone. Frontiers in endocrinology. 2015:162.
31. Francisco JI, Yu Y, Oliver RA, Walsh WR. Relationship between age, skeletal site, and time post-ovariectomy on bone mineral and trabecular microarchitecture in rats. Journal of Orthopaedic Research. 2011;29(2):189-96.
32. Mathavan N, Turunen MJ, Tägil M, Isaksson H. Characterising bone material composition and structure in the ovariectomized (OVX) rat model of osteoporosis. Calcified tissue international. 2015;97(2):134-44.
33. Choi HK, Kim G-J, Yoo H-S, Song DH, Chung K-H, Lee K-J, et al. Vitamin C Activates Osteoblastogenesis and Inhibits Osteoclastogenesis via Wnt/β-Catenin/ATF4 Signaling Pathways. Nutrients. 2019;11(3):506.
34. Lee YM, Kim IS, Lim BO. Black rice (Oryza sativa L.) fermented with Lactobacillus casei attenuates osteoclastogenesis and ovariectomy-induced osteoporosis. BioMed research international. 2019;2019.
35. Wronski T, Cintron M, Dann L. Temporal relationship between bone loss and increased bone turnover in ovariectomized rats. Calcified tissue international. 1988;43(3):179-83.
36. Keiler AM, Zierau O, Vollmer G, Scharnweber D, Bernhardt R. Estimation of an early meaningful time point of bone parameter changes in application to an osteoporotic rat model with in vivo microcomputed tomography measurements. Laboratory animals. 2012;46(3):237-44.
37. Baim S, Miller PD. Perspective: assessing the clinical utility of serum CTX in postmenopausal osteoporosis and its use in predicting risk of osteonecrosis of the jaw. Journal of bone and mineral research. 2009;24(4):561-74.
38. Wronski T, Schenk P, Cintron M, Walsh C. Effect of body weight on osteopenia in ovariectomized rats. Calcified tissue international. 1987;40(3):155-9.
39. Skowrońska-Jóźwiak E, Jaworski M, Lorenc R, Karbownik-Lewińska M, Lewiński A. Low dairy calcium intake is associated with overweight and elevated blood pressure in Polish adults, notably in premenopausal women. Public health nutrition. 2017;20(4):630-7.
40. Booth AO, Huggins CE, Wattanapenpaiboon N, Nowson CA. Effect of increasing dietary calcium through supplements and dairy food on body weight and body composition: a meta-analysis of randomised controlled trials. British Journal of Nutrition. 2015;114(7):1013-25.
41. Bourrat X, Francke L, Lopez E, Rousseau M, Stempflé P, Angellier M, et al. Nacre biocrystal thermal behaviour. CrystEngComm. 2007;9(12):1205-8.
42. Gala J, Di M, de la Piedra C. Short-and long-term effects of calcium and exercise on bone mineral density in ovariectomized rats. British Journal of Nutrition. 2001;86(4):521-7.
43. Ben Ammar R, Piet MH, Brion A, Telahigue K, Werheni R, Rousseau M, et al. Induction of Osteogenic MC3T3-E1 Cell Differentiation by Nacre and Flesh Lipids of Tunisian Pinctada radiata. Lipids. 2019;54(8):433-44.
44. Harvey JA, Zobitz MM, Pak CY. Dose dependency of calcium absorption: a comparison of calcium carbonate and calcium citrate. Journal of Bone and Mineral Research. 1988;3(3):253-8.
45. Iki M, Akiba T, Matsumoto T, Nishino H, Kagamimori S, Kagawa Y, et al. Reference database of biochemical markers of bone turnover for the Japanese female population. Japanese Population-based Osteoporosis (JPOS) Study. Osteoporosis international. 2004;15(12):981-91.

46. Ben-Dov IZ, Galitzer H, Lavi-Moshayoff V, Goetz R, Kuro-o M, Mohammadi M, et al. The parathyroid is a target organ for FGF23 in rats. The Journal of clinical investigation. 2007;117(12):4003-8.
47. Carrillo-López N, Román-García P, Rodríguez-Rebollar A, Fernández-Martín JL, Naves-Díaz M, Cannata-Andía JB. Indirect regulation of PTH by estrogens may require FGF23. Journal of the American Society of Nephrology. 2009;20(9).
48. Thompson D, Simmons H, Pirie C, Ke H. FDA Guidelines and animal models for osteoporosis. Bone. 1995;17(4):S125-S33.

Figures and figure legends

Figure 1. The changes of morphological trabecular bone from baseline (start point - D0) to follow-up (end point - D28) in the proximal tibia in *in vivo* longitudinal study. µCT scout-view image, in which the box depicts a scanned region of 147 consecutive slices (15 µm/slice) analyzed for trabecular bone volume, as detailed in Methods (**A**). Percent changes in BV/TV, Conn.D and Tb.Th in OVX groups compared to Sham **(B)**. Representative 3-dimensional (3D) µCT images of the proximal tibial metaphysis of an animal (median from each group) at day 0 and day 28 (**C**)**.** Data represent the change of baseline-adjusted mean groups relative to Sham in % (n=10 per group). ** P ≤ 0.01, *** P ≤ 0.001, * *vs.* Sham (ANCOVA generalized linear model using values at baseline as covariable described in the text). The raw data (right column) show the mean, and 95% CIs used for ANCOVA analysis, which provide F ($df_{between}$, df_{within}) = Test Statistic, P values of the group effect whilst adjusting for baseline and effect size generalized eta squared (η_g^2).

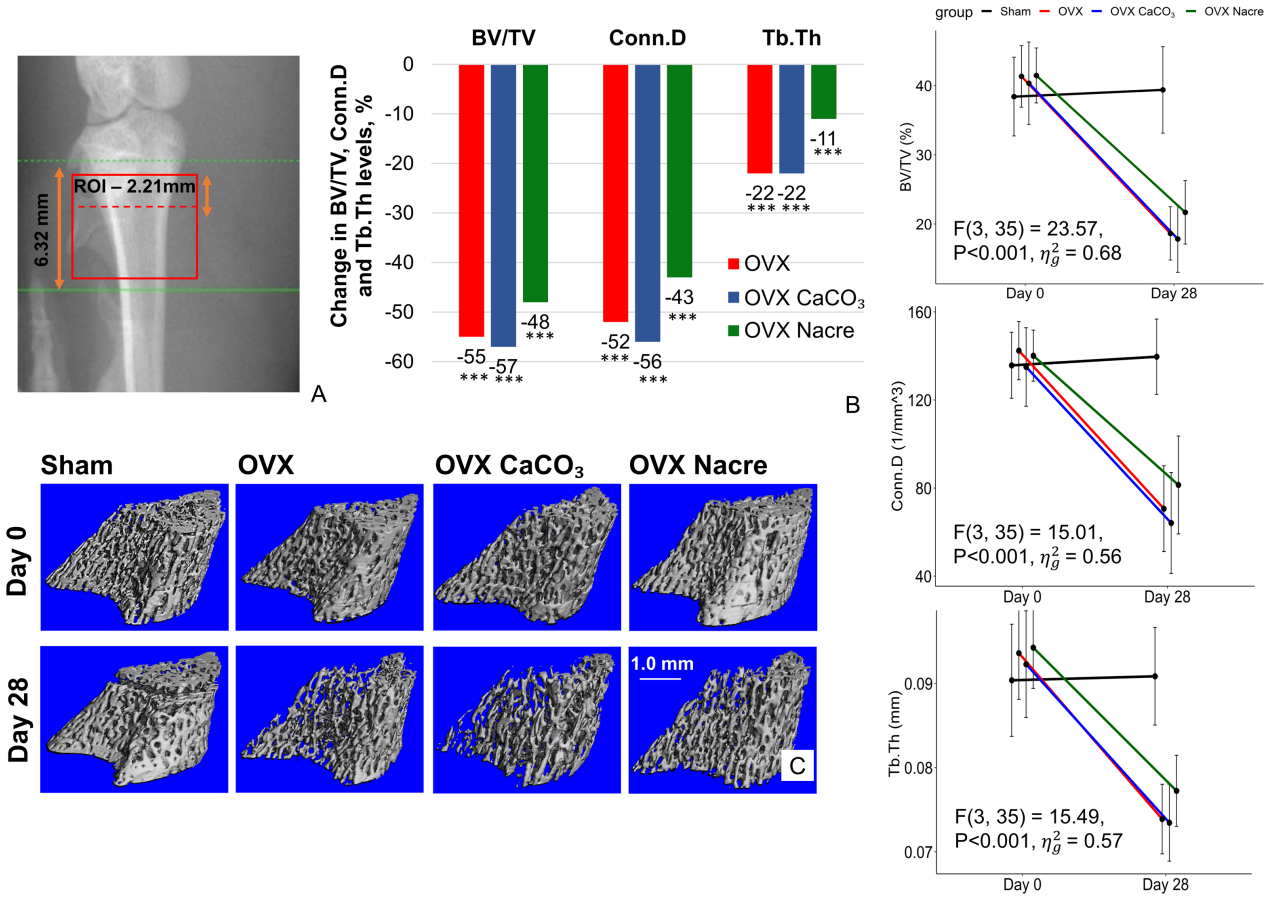

Figure 2. **The morphological trabecular parameters in the distal metaphyseal femur in *ex vivo* cross-sectional micro-computed tomography (μCT) study**. μCT scout image, in which the box depicts a scanned region of 147 consecutive slices (10.5 μm/slice) analyzed for trabecular bone volume, as detailed in Methods (**A**). Representative 3-dimensional images of the trabecular bone microarchitecture in the right distal femur **(B)**. Percent changes in BV/TV, Conn.D and Tb.Th in OVX groups compared to Sham group **(C)**. Data represent the change of median OVX groups relative to Sham in % (n=10 per group). * $P \leq 0.05$, ** $P \leq 0.01$, *** $P \leq 0.001$; * *vs.* Sham group, $^{\#}$ *vs.* OVX group, $^{\$}$ *vs.* OVX $CaCO_3$ group (Kruskal-Wallis test followed by Mann-Whitney-Wilcoxon unpaired test with Benjamini-Hochberg adjustment). Sample distributions were shown in Figure S3.

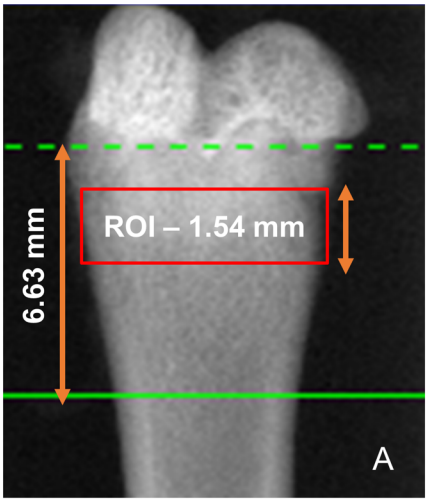
6.63 mm
ROI – 1.54 mm
A

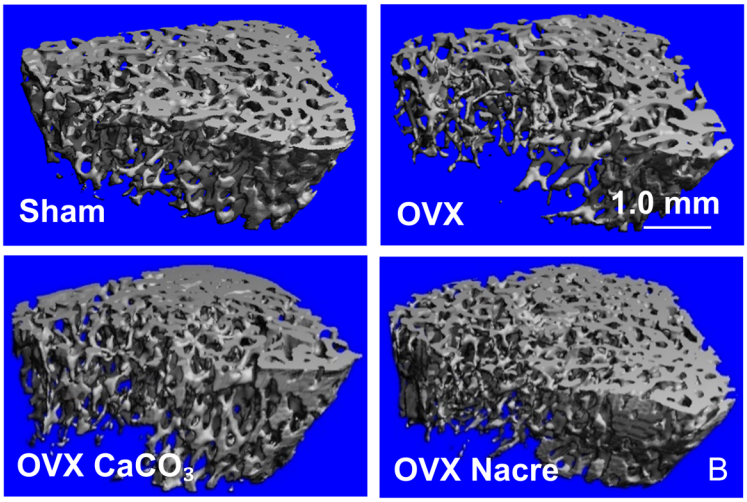
Sham
OVX
1.0 mm
OVX CaCO3
OVX Nacre
B

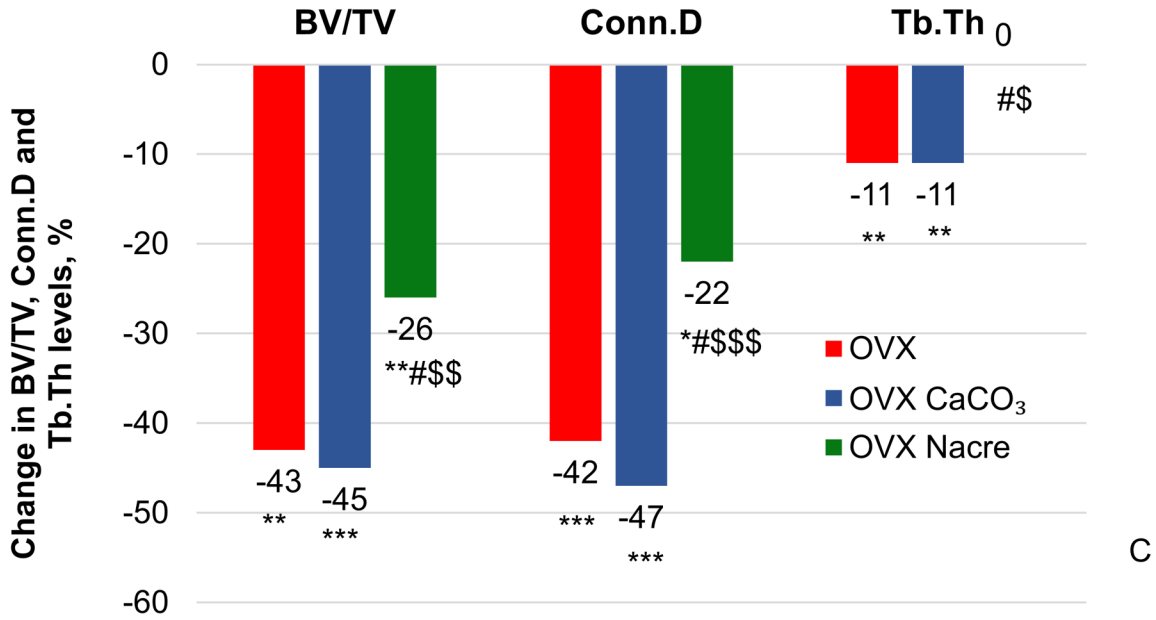
BV/TV
Conn.D
Tb.Th
0
-10
-20
-30
-40
-50
-60
Change in BV/TV, Conn.D and Tb.Th levels, %
-43
**
-45
***
-26
**#$$
-42
***
-47
***
-22
*#$$$
-11
**
-11
**
#$
OVX
OVX CaCO3
OVX Nacre
C

Figure 3. **The histomorphometric characteristics in the undecalcified proximal metaphyseal tibia through 9 µm sections at day 28**. Representative sections stained with Goldner's trichrome **(A)**. They show full longitudinal sections of median animals in each group and the ROI for histomorphometry measurements is outlined in yellow, magnification x5, scale bar = 1 mm. The bone volume fraction (BV/TV) derived from sections stained with Goldner's **(B)**. Representative sections stained with tartrate – resistant acid phosphate (TRAcP) **(C)**. The red arrows indicate red-stained osteoclasts, magnification x20, scale bar = 250 µm. The osteoclast surface per bone surface parameter (Oc.S/BS) derived from sections stained with TRAcP **(D)**. Data represent as boxplots, and show all data points, with interquartile range (IQR) (height of the box), median (internal horizontal bar) n = 9 per Sham / OVX $CaCO_3$ group; n = 10 per OVX / OVX Nacre group), mean (black filled square, ■). * $P \leq 0.05$, ** $P \leq 0.01$, *** $P \leq 0.001$; * *vs.* Sham, $^{\#}$ *vs.* OVX, $^{\$}$ *vs.* OVX $CaCO_3$ (Kruskal-Wallis test followed by Mann-Whitney-Wilcoxon unpaired test with Benjami-Hochberg adjustment).

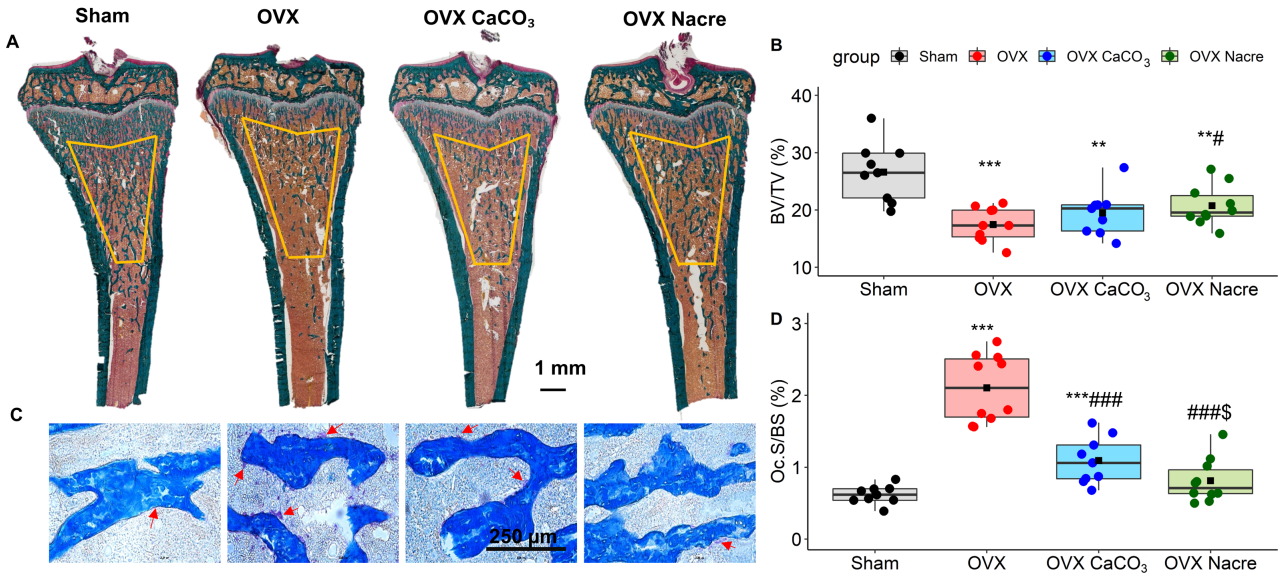

Figure 4. Principal Component Analysis (PCA) in the tibia for trabecular variables measured by µCT and histomorphometry. Biplot includes Score plots that represents the distribution of individual rats in the space defined by Principal Component 1 (PC1) and PC2, and Loading plots that represents the contribution of each variable, corresponding to each loading vector in the space defined by PC1 and PC2. The weights of loading vectors in each PC are shown in the right panel. n = 9 per Sham / OVX $CaCO_3$ group; n = 10 per OVX / OVX Nacre group.

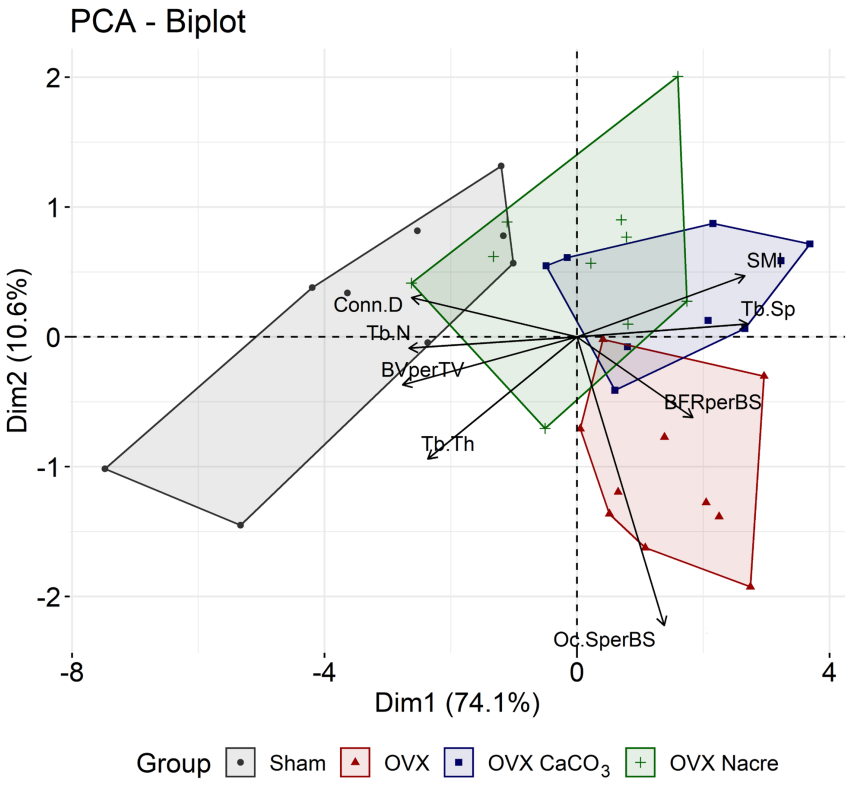

	PC1	PC2
BVperTV	-0.40	-0.14
Conn.D	-0.38	0.12
SMI	0.39	0.18
Tb.N	-0.39	-0.03
Tb.Th	-0.35	-0.36
Tb.Sp	0.39	0.04
Oc.SperBS	0.20	-0.86
BFRperBS	0.27	-0.24

Figure 5. mRNA expression levels of genes involved in bone formation (A) and bone resorption (B) using extracts from flushed marrow (ma) or bone fraction at day 28. Transcript levels were normalized to house-keeping gene *Hprt1* following the $2^{(-\Delta\Delta C(t))}$ method [24]. The specific primers (based on the rat sequences) are displayed in Table S1. Data represent as boxplots, and show all data points, with interquartile range (IQR) (height of the box), median (internal horizontal bar) (n=10 per group), mean (black filled square, ■). * $P \leq 0.05$, ** $P \leq 0.01$, *** $P \leq 0.001$; * *vs*. Sham, # *vs*. OVX, $ *vs*. OVX $CaCO_3$ (ANOVA test followed by Tukey's HSD post-hoc test or Kruskal-Wallis test followed by Mann-Whitney-Wilcoxon unpaired test with Benjami-Hochberg adjustment). *Hprt1* = hypoxanthine phosphoribosyltransferase 1.

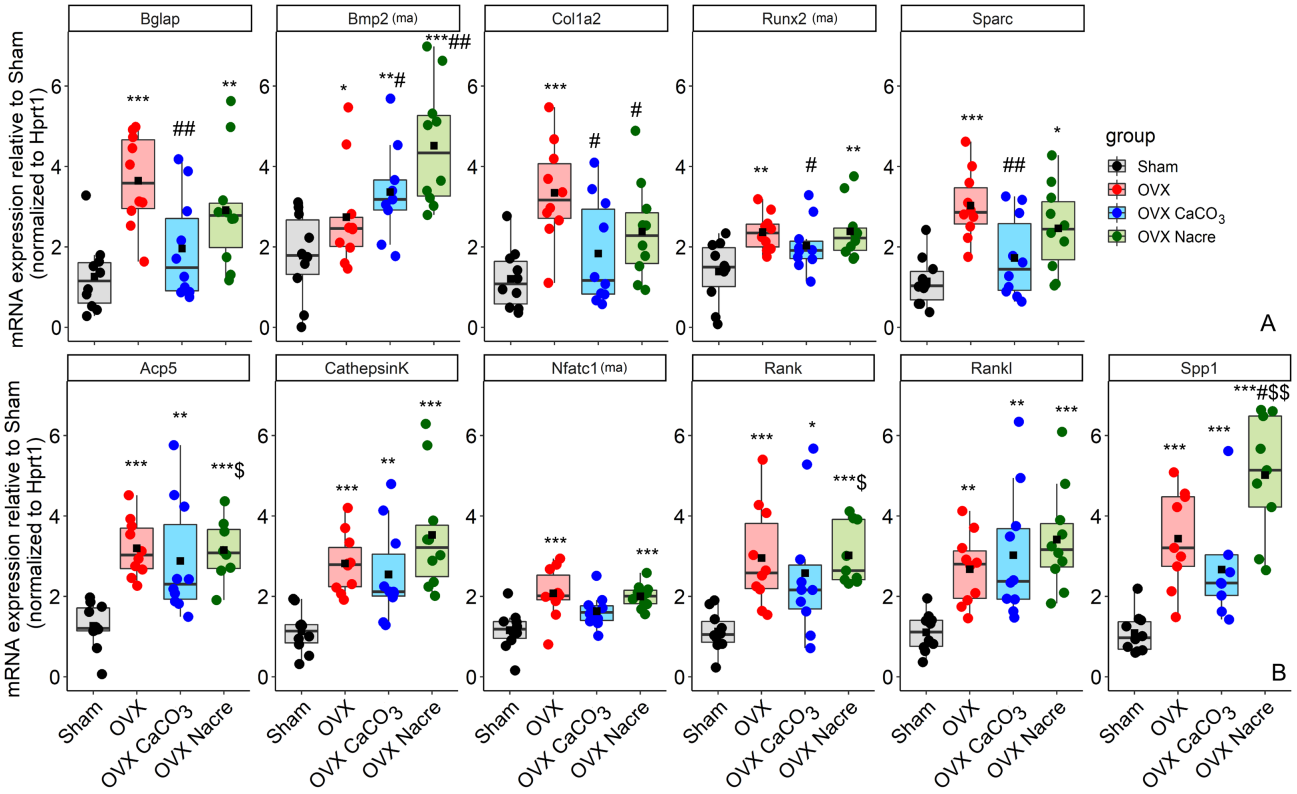

Figure 6. Changes of serum bone turnover markers from baseline (day 0) to follow-ups in the Sham and OVX rats. The data were represented as the mean ± standard error (vertical bar) (n=6 per group). P-values indicated the effect of group (between-subjects factor) and / or time (within-subjects factor) and the group x time interaction using two-way repeated measures ANOVA, followed by Tukey's HSD post-hoc test to adjust for multiple comparisons. $^{\#}$ $P \leq 0.05$, $^{\#\#}$ $P \leq 0.01$, $^{\#\#\#}$ $P \leq 0.001$, * *vs.* Sham, $^{\#}$ *vs.* OVX, $^{\$}$ *vs.* OVX $CaCO_3$; $^{£}$ *vs.* baseline at day 0, $^{¤}$ *vs.* follow-up at day 14.

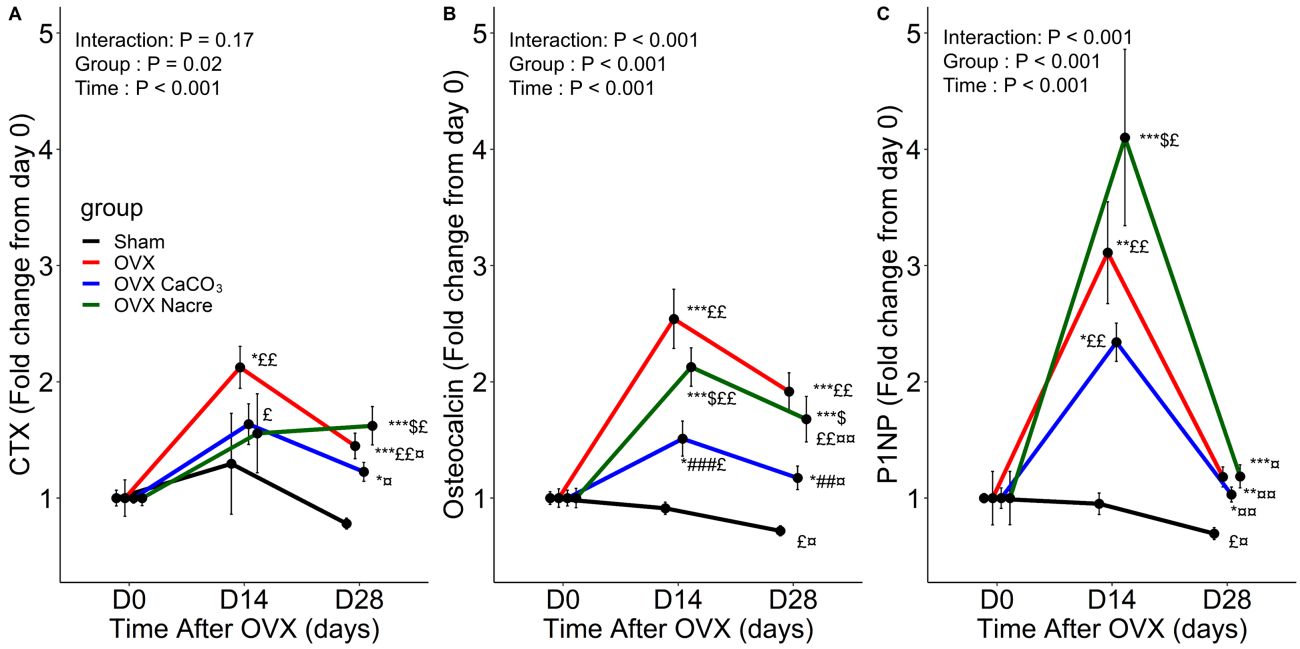

Table 1. Trabecular bone morphology at baseline and follow-up in the proximal tibiae in the Sham and OVX rats (*in vivo* longitudinal study).

Characteristic (unit)	Estimate	Group			
		Sham	OVX	OVX $CaCO_3$	OVX Nacre
BV/TV (%)	Baseline	38.42 (7.95)	41.34 (6.21)	40.34 (8.33)	41.47 (5.56)
	Follow-up	39.39 (8.73)	18.64 (5.37)	17.84 (6.73)	21.69 (6.41)
	Adjusted follow-up	41.3	18.5 ***	17.8 ***	21.4 ***
Conn.D ($1/mm^3$)	Baseline	135.75 (20.96)	142.42 (18.54)	134.99 (24.92)	140.13 (16.22)
	Follow-up	139.68 (23.88)	70.64 (27.25)	64.14 (32.0)	81.42 (31.06)
	Adjusted follow-up	142.2	68.0 ***	63.2 ***	81.2 ***
Tb.N (1/mm)	Baseline	5.17 (0.53)	5.37 (0.44)	5.28 (0.62)	5.37 (0.33)
	Follow-up	5.24 (0.60)	3.87 (0.60)	3.71 (0.79)	4.20 (0.68)
	Adjusted follow-up	5.37	3.82 ***	3.71 ***	4.17 **
Tb.Th (mm)	Baseline	0.09 (0.01)	0.09 (0.01)	0.09 (0.01)	0.09 (0.01)
	Follow-up	0.09 (0.01)	0.07 (0.01)	0.07 (0.01)	0.08 (0.01)
	Adjusted follow-up	0.09	0.07 ***	0.07 ***	0.08 ***
Tb.Sp (mm)	Baseline	0.16 (0.03)	0.15 (0.02)	0.16 (0.03)	0.15 (0.01)
	Follow-up	0.16 (0.03)	0.25 (0.05)	0.27 (0.09)	0.22 (0.04)
	Adjusted follow-up	0.15	0.25 **	0.27 ***	0.23*
SMI®	Baseline	0.68 (0.86)	0.52 (0.60)	0.50 (0.74)	0.52 (0.62)
	Follow-up	0.55 (0.90)	2.38 (0.32)	2.40 (0.38)	2.24 (0.43)
	Adjusted follow-up	0.45	2.38 ***	2.40 ***	2.24 ***

Note: Microarchitectural parameters were adjusted for individual values at Baseline (Start point) by using the analysis of covariance generalized linear model described in the text.

* P ≤ 0.05, ** P ≤ 0.01, *** P ≤ 0.001; * *vs*. Sham.

®For the structure model index: 0 parallel plates, 3 cylindrical rods, and 4 spheres

Values are mean (standard deviation), n=10 per group.

Table 2. µCT-derived trabecular bone microarchitectural parameters in the second lumbar spine (LS2) in *ex vivo* cross-sectional study.

Characteristic (unit)	Group				P-value †
	Sham	OVX	OVX $CaCO_3$	OVX Nacre	
BV/TV	0.41 (0.37 - 0.42)	0.36* (0.35 - 0.39)	0.35** (0.34 - 0.35)	0.39$^{\#\$\$}$ (0.38 - 0.41)	**0.01**
Conn.D (1/mm³)	102.28 (88.38 - 106.24)	87.87 (85.35 - 96.85)	90.19 (84.24 - 92.17)	88.98 (79.97 - 94.33)	>0.10
Tb.N (1/mm)	4.79 (4.60 - 5.02)	4.50** (4.39 - 4.57)	4.25***$^{\#}$ (4.20 - 4.39)	4.45*$^{\$}$ (4.35 - 4.64)	**0.001**
Tb.Th (mm)	0.08 (0.08 - 0.09)	0.08 (0.08 - 0.08)	0.08 (0.08 - 0.08)	0.09 (0.08 - 0.09)	>0.10
Tb.Sp (mm)	0.18 (0.17 - 0.19)	0.20* (0.19 - 0.20)	0.21**$^{\#}$ (0.20-0.22)	0.20*$^{\$}$ (0.19 - 0.20)	**0.001**
SMI®	-0.74 (-0.84 - -0.16)	-0.29* (-0.44 - -0.12)	-0.21 (-0.30 - -0.01)	-0.52 (-0.73 - -0.39)	**0.03**

Note: †Kruskal Wallis test

Post-hoc pairwise comparisons were conducted using Mann-Whitney-Wilcoxon (MWW) unpaired tests with Benjamini-Hochberg adjustment.

P-values in bold indicated statistical significance at a level of 5% ($P \leq 0.05$).

*$P \leq 0.05$, **$P \leq 0.01$, ***$P \leq 0.001$; * *vs.* Sham, $^{\#}$ *vs.* OVX, $^{\$}$ *vs.* OVX $CaCO_3$.

®For the structure model index, 0 indicates parallel plates, 3 cylindrical rods, and 4 spheres

Values are median (interquartile range), n=10 per group.

Table 3. Summary of representative parameters of trabecular bone analysis in different skeletal sites using *ex vivo* µCT.

Bone site	Trabecular parameters	OVX Nacre *vs*. OVX ($^{\#}$)	OVX Nacre *vs*. OVX $CaCO_3$ ($^{\$}$)
Femoral distal metaphysis	BV/TV	0.07 (**0.04**$^{\#}$)	0.08 (**0.004**$^{\$\$}$)
	Tb.Th (mm)	0.01 (0.10)	0.01 (**0.03**$^{\$}$)
	Tb.N (1/mm)	0.54 (**0.03**$^{\#}$)	0.93 (**0.002**$^{\$\$}$)
	Tb.Sp (mm)	-0.03 (**0.05**$^{\#}$)	-0.07 (**0.002**$^{\$\$}$)
2nd lumbar spine (LS2)	BV/TV	0.03 (**0.04**$^{\#}$)	0.04 (**0.01**$^{\$\$}$)
	Tb.Th (mm)	0.01 (>0.10)	0.01 (>0.10)
	Tb.N (1/mm)	-0.05 (>0.10)	0.20 (**0.03**$^{\$}$)
	Tb.Sp (mm)	0.00 (>0.10)	-0.01 (**0.02**$^{\$}$)
Tibial proximal metaphysis	BV/TV	0.01 (0.09)	0.06 (0.07)
	Tb.Th (mm)	0.01 (>0.10)	0.01 (**0.05**$^{\$}$)
	Tb.N (1/mm)	0.18 (>0.10)	0.52 (**0.01**$^{\$\$}$)
	Tb.Sp (mm)	0.00 (>0.10)	-0.02 (**0.05**$^{\$}$)

Note: Data were represented as the difference of median and P-values in brackets () using Mann-Whitney-Wilcoxon unpaired tests with Benjamini-Hochberg adjustment. P-values in bold indicated statistical significance at a level of 5% ($P \leq 0.05$).

$^{\#}$ $P \leq 0.05$; $^{\#\#}$ $P \leq 0.01$; $^{\#}$ *vs*. OVX, $^{\$}$ *vs*. $CaCO_3$

Table 4. Histomorphometry of trabecular bone in the proximal tibiae of Sham and OVX rats.

Type of index (unit)	Group (No. of rats)				
	Sham (9)	OVX (10)	OVX $CaCO_3$ (9)	OVX Nacre (10)	
Static indices					**P-value †**
N.Oc/B.Ar (c/mm²)	38.99 (36.21 - 43.10)	122.11*** (103.22 - 133.25)	68.60**### (44.76 - 75.39)	46.11### (42.02 - 62.08)	**<0.001**
N.Oc/B.Pm (c/mm)	0.80 (0.76 - 0.85)	2.41*** (2.16 - 2.71)	1.44**## (1.03 - 1.64)	0.98### (0.78 - 1.34)	**<0.001**
Oc.S/BS (%)	0.62 (0.54 - 0.70)	2.11*** (1.70 - 2.51)	1.06***### (0.84 - 1.31)	0.71###$ (0.63 - 0.97)	**<0.001**
Oc.Le (µm)	15.82 (15.33 - 17.52)	19.38 (16.34 - 18.97)	16.94 (15.34 - 18.01)	16.30 (15.14 - 17.41)	>0.10
Dynamic indices					
sLS/BS (%)	1.97 (1.77 - 2.40)	6.29** (3.51 - 8.19)	6.17*** (3.87 - 6.93)	5.42*** (4.71 - 5.89)	**<0.001**
dLS/BS (%)	0.70 (0.53 - 1.23)	4.22** (3.38 - 5.86)	4.23* (0.67 - 6.47)	3.62 (1.32 - 5.09)	**0.02**
MAR (µm/day)	1.34 (1.29 - 1.49)	1.44 (1.01 - 1.62)	1.74# (1.63 - 1.91)	1.45*$ (1.36 - 1.52)	**0.04**
MS/BS (%)	1.74 (1.32 - 2.60)	7.73*** (5.39 - 9.37)	6.07*** (4.26 - 9.56)	6.17*** (2.32 - 7.73)	**<0.001**
BFR/BS ($\mu m^3/\mu m^2$/day)	3.12 (2.84 - 3.76)	9.20*** (6.30 - 10.91)	7.81*** (6.94 - 11.37)	7.68*** (4.97 - 9.24)	**<0.001**

Note: †Kruskal Wallis test

Post hoc pairwise comparisons were conducted using Mann-Whitney-Wilcoxon unpaired tests with the Benjamini-Hochberg adjustment.

P-values in bold indicated statistical significance at a level of 5% ($P \leq 0.05$).

*P ≤ 0.05, **P ≤ 0.01, ***P ≤ 0.001; * *vs.* Sham, # *vs.* OVX, $ *vs.* OVX $CaCO_3$.

Values are median (interquartile range).

N.OC/B.Ar, number osteoclast per bone area; N.Oc/B.Pm, number osteoclast per bone perimeter; Oc.S/BS, osteoclast surface par bone surface; Oc.Le, osteoclast length; sLS/BS, single-labeled surface per bone surface; dLS/BS, double-labeled surface per bone surface; MAR, mineral apposition rate; MS/BS, mineralizing surface per bone surface; BFR/BS, bone formation rate per bone surface.

Supplemental Materials

Protective effect on bone of nacre supplementation in ovariectomized rats

Dung Kim NGUYEN [1], Norbert LAROCHE [1], Arnaud VANDEN-BOSSCHE [1], Marie-Thérèse LINOSSIER [1], Mireille THOMAS [1], Sylvie PEYROCHE [1], Myriam NORMAND [1], Yacine BERTACHE [1], Thierry THOMAS [1,2], Hubert MAROTTE [1,2], Laurence VICO [1], Marie-Hélène LAFAGE-PROUST [1,2], Marthe ROUSSEAU [1,3]

Section 1: **Microarchitectural analysis description by using µCT**.

For *in vivo* µCT evaluation, cortical dimensions were determined on the last 58 slices (0.87mm) to obtain cross-sectional images for the volume of interest (VOI) drawn to exclude trabecular elements. Cortical analyses were measured at a threshold of 260 mg/cm^3, a Gaussian filter (sigma = 0.8, support = 1). Trabecular bone measurements at the proximal tibiae were made on 147 slices (2.21mm) away from the growth plate, to avoid the primary spongiosa. Trabecular bone analyses were performed on the contours of the cross-sectional images drawn to exclude cortical bone and were measured at a threshold of 190mg/cm^3, a Gaussian filter (sigma=1 and support=2). Both metric and non-metric bone parameters were evaluated. Metric parameters included: (i) trabecular bone morphometry: bone volume fraction (BV/TV, %); trabecular number (Tb.N, 1/mm); trabecular separation (Tb.Sp, mm); trabecular thickness (Tb.Th, mm); connectivity density (Conn.D, 1/mm^3); (ii) cortical bone morphometry: cortical bone area (Ct.Ar, mm²); cortical thickness (Ct.Th, mm); marrow area (Ma.Ar, mm²), cortical porosity (Ct.Po, %). Non-metric parameters included the Structure Model Index (SMI), where an ideal value of 0 indicates the predominance of plate-like structure, while a value of 3 indicates

the predominance of rod-like structure. Nomenclature conforms to recommendations of the American Society for Bone and Mineral Research [(1)].

For *ex vivo* μCT analyses of different skeletal sites. All bone tissues (tibiae, femora, lumbar spine) were placed in a tube filled with alcohol, blocked by the cotton plug, and scanned. Scan settings were as follows: isotropic voxel size 10.5 μm^3, 70kVp, 114μA, 1000 projections by 180 degrees with 250 ms integration time. The information on the scanning system and the VOI's dimension in detail were indicated in Tab. S2. Figures 2A and S4 were given to illustrate the scout-view, drawn ROI, and representative 3D images of VOI.

The second lumbar spine (LS2) was scanned between 2 discs to obtain 619 slices (6.50 mm). Trabecular parameters in the spine were determined using 347 slices (3.64 mm) centered at the body of LS2. Trabecular bone analyses were performed on contours of cross-sectional images, drawn to exclude cortical bone, as described for femoral trabecular bone.

Section 2: Bone histomorphometry measurements

After μCT scanning, the right tibiae were trimmed of soft tissue and fixed at 4°C with 70% ethanol for 14 days. The proximal one-third of the tibiae were cut, then embedded undecalcified in methyl methacrylate (MMA) following dehydration in 100% ethanol. Because of technical reasons, we lost 1 sample in each Sham and OVX $CaCO_3$ group. Thus, we performed these histomorphometric measurements with sample sizes as n=9/ Sham o**r** VX $CaCO_3$ group, n=10/ OVX, or OVX Nacre group. Nine μm-thick frontal sections for staining and 12 μm - thick sections for dynamic analysis were cut using a microtome (SM2500; Leica Biosystems Nussloch GmbH, Germany) and mounted on slides. The 9 μm – thick sections were stained with Goldner's trichrome and tartrate-resistant acid phosphatase (TRAcP) to assess the microstructure and visualize osteoclasts, respectively. Unstained 9 μm – thick sections were analyzed using a fluorescence microscope (Zeiss Axio Scope A1, Germany) to determine the dynamic indices of bone formation based on tetracyclinlabelingng. Structural and dynamic histomorphometry indices were measured in the trabecular bone of the secondary spongiosa, using a semi-automatic image analysis system (Sony DXC 950P Camera; DMRB microscope, Leica

Microsystems, Germany; Explora Nova software version 3.50, La Rochelle, France) at a magnification x 5 for microstructural indices and x 20 for cellular and dynamic indices. The primary static indices included bone volume fraction (BV/TV, %), trabecular thickness (Tb.Th, µm), trabecular number (Tb.N, 1/mm), trabecular separation (Tb.Sp, µm), Osteoclast Number per Bone Area (N.Oc/B.Ar, mm^2), Osteoclast Number per Bone perimeter (N.Oc/B.Pm, c/mm), Osteoclast Surface per Bone Surface (Oc.S/BS, %), Osteoclast Length (Oc.Le, µm). The dynamic parameters obtained from the tetracycline marker included single-labeled surface per bone surface (sLS/BS, %), and double-labeled surface per bone surface (dLS/BS, %). Mineral Apposition Rate (MAR, µm/day) was calculated from the mean distance between the labels divided by the number of days between labelings. Mineralizing Surface per Bone Surface (MS/BS, %) was calculated as ½ sLS/BS + dLS/BS. Bone - Formation Rate per Bone Surface (BFR/BS, $\mu m^3/\mu m^2$/day) was calculated by multiplying MS/BS by MAR. The histomorphometry nomenclature used in the present study was from a report from the American Society for Bone and Mineral Research Histomorphometry Nomenclature Committee [(2)].

Section 3: Supplemental tables.

Table S1. Composition of experimental diets.

Composition	Standard	OVX		
		Standard	$CaCO_3$ supplement	Nacre supplement
	Sham †	OVX †	OVX $CaCO_3$ ‡	OVX Nacre ‡
Acid amin Mix (g/kg) [a]	21.5	21.5	21.5	>21.5*
Fat acid Mix (g/kg) [b]	19.8	19.8	19.8	>19.8*
Vitamin Mix (g/kg) [c]	1.72	1.72	1.72	1.72
Soya trace	free	free	free	free
Mineral Mix (g/kg) [d]	27.84	27.84	28.84	28.79
Calcium included	8.5	8.5	9.5	9.45

Note: † Sham and OVX groups = standard diet, ‡ OVX $CaCO_3$ and OVX Nacre groups = standard diet supplemented with 0.25% $CaCO_3$ or nacre powder, respectively.

**Pinctata maxima*'s nacre contains 2.7% organic matrix (Bourrat X et al., *CrysEngComm*, 2007 [(3)]) ; 0.068 g nacre organic content per 1kg food.

[a] acid amin Mix – Arginine : 6.5, Cysteine : 2, Lysine : 4.4, Methionine : 1.8, Tryptophane : 1.5, Glycine : 5.3

[b] Fat acid Mix – Palmitic acid : 2.2, Stearic acid : 0.4, Oleic acid : 6, Linoleic acid : 11.2, Linolenic acid : 0.4

[c] Mineral Mix – Phosphate : 5, Sodium : 2.2, Potassium : 6.3, Magnesium : 1.9, Maganese : 0.09, Fer : 0.27, Copper : 0.016, Zinc : 0.060, Chlorure : 3.5

[d] Vitamine Mix – Vit A : 5, Vit D3 : 9, Vit B1 : 0.005, vit B2 : 0.006, Vit B5 : 0.01, vit B6 : 0.002, vit B12 : 2.10^{-5}, vit E : 0.025, vit K3 : 0.0025, Niacine : 0.07, acid Folic : 0.0005, Biotine : 0.00004, Choline : 1.6

Table S2. **The supplemental information used in bone morphology analysis by µCT.**

Bone site	**Voxel size (μm^3)**	**Gaussian filter**		**Threshold (mg/cm^3)**	**Dimension (mm)**		**Type of study**	
		Sigma	**Support**		**Acquisition**	**Evaluation**	***In vivo***	***Ex vivo***
Trabecular proximal tibia	15	1	2	190	6.32 [421]	2.21 [147]	x	
Cortical proximal tibia	15	0.8	1	260	6.32 [421]	0.87 [58]	x	
Trabecular proximal tibial metaphysis	10.5	1	2	190	4.42 [421]	1.54 [147]		x
Cortical tibial diaphysis	10.5	0.8	1	260	2.22 [211]	0.62 [59]		x
Trabecular distal femoral metaphysis	10.5	1.5	2	290	6.63 [631]	1.54 [147]		x
Cortical femoral diaphysis	10.5	0.8	1	260	2.15 [205]	0.91 [87]		x
Trabecular 2nd lumbar spine	10.5	1.2	2	240	6.50 [619]	3.64 [347]		x

Note: The number of slices was indicated in square brackets [].

Table S3. Primer sequences used in this study

Genes (protein encoded)	**Sense (5'-3')**	**Antisense (5'-3')**
Hprt1	GTTGGATACAGGCCAGACTT	GCCACATCAACAGGACTCTT
Runx2 (RUNX2)	CAGACCAGCAGCACTCCATA	CGCCAGACAGACTCATCCAT
Bglap (Osteocalcin)	CAACTCGGTGCAGACCTAGC	GAGGTAGCGCCGGAGTCTAT
Spp1 (Osteopontin)	GGAGAAGGCGCATTACAGCA	CGTCATCGTCGTCGTCATCA
Sparc (Osteonectin)	AGGTGTGCAGCAATGACAAC	ATTCGGTCAGCTCAGAATCC
Col1a2 (Collagen type 1 α2)	ATTGCGTACCTGGACGAGGA	GGCAGGCGAGATGGCTTATT
Bmp2 (BMP-2)	TTGAGGCTGCTCAGCATGTT	CTCGATGGCTTCTTCGTGAT
Nfatc1 (NFATc1)	CGTGGAGAAGCAGAGCACAG	CTTGCACAGGTCTCGGTCAG
Acp5 (TRAP)	CAGCCAAGGAGGACTATGTT	ACACCGTTCTCATCCTGAAG
Cathepsin K (Cathepsin K)	AGTGCCACCTTCGCGTTCCT	TAGCCGCCTCCACAGCCATA
Rank (RANK)	ATCGTCCTGCTCCTCTTCAT	ACTTCTTGCTGGCTGGAGTT
Rankl (RANKL)	GACAGCACGCGCTGCTTCTA	CCACATCGAGCCACGAACCT

Table S4. Quantification of µCT-derived cortical bone microarchitectural parameters at the tibial and femoral diaphysis in *ex vivo* cross-sectional study.

Characteristic (unit)	Tibial diaphysis					Femoral diaphysis				
	Group					Group				
	Sham	OVX	OVX $CaCO_3$	OVX Nacre	P-value†	Sham	OVX	OVX $CaCO_3$	OVX Nacre	P-value †
Ct.Ar (mm²)	3.70 (3.64-3.73)	3.97*** (3.82-4.05)	4.04 (3.64-4.14)	3.98** (3.90-4.13)	**0.02**	5.21 (4.96-5.34)	5.60* (5.52-5.65)	5.50 (5.29-5.86)	5.43* (5.24-5.72)	0.06
Ct.Th (mm)	0.55 (0.53-0.56)	0.56 (0.51-0.59)	0.57 (0.55-0.59	0.57 (0.55-0.59)	>0.10	0.61 (0.60-0.62)	0.62 (0.61-0.63)	0.60 (0.59-0.62)	0.60 (0.58-0.63)	>0.10
Ma.Ar (mm²)	1.39 (1.26-1.48)	1.41 (1.29-1.48)	1.43 (1.29-1.55)	1.51 (1.24-1.78)	>0.10	2.86 (2.57-3.90)	2.96 (2.70-3.32)	3.16 (2.61-3.38)	2.96 (2.77-3.43)	>0.10
Ct.Po (%)	2.91 (2.85-3.03)	3.36 (3.10-3.58)	3.12 (2.95-3.40)	3.10 (3.06-3.35)	0.06	1.30 (1.23-1.32)	1.42 (1.29-1.48)	1.44 (1.39-1.55)	1.39* (1.26-1.59)	>0.10

Note: †Kruskal Wallis test

Post hoc pairwise comparisons were conducted using Mann-Whitney-Wilcoxon unpaired tests with the Benjamini-Hochberg adjustment.

P-values in bold indicated statistical significance at level of 5% (P ≤ 0.05). *P ≤ 0.05, **P ≤ 0.01, ***P ≤ 0.001; * *vs*. Sham, # *vs*. OVX.

Values are median (interquartile range), n=10 per group

Section 4: Supplemental figure legends

Figure S1. **OVX-induced body weight variation in rats**. The rat growth (weight, g) before and after the ovariectomized surgery (occurred at week 16 – Day 0) **(A)**. Data represent mean ± standard error (n=10 per group). † P-values were derived from a one-way ANOVA test. The body weight changes from baseline (Day 0) during 28 days of study **(B)**. The symmetric percent changes were calculated by finding the individual difference of values at baseline (*x0*) and follow-ups (D14 or D28) (*x1*), then divided this difference by the mean of baseline and follow-up values, i.e *(x1-x0)/mean (x0, x1) x 100.* Data represent mean ± standard error (n=10 per group). *** $P \leq 0.001$ *vs.* Sham; $^{\#}$ $P \leq 0.05$, $^{\#\#\#}$ $P \leq 0.001$ *vs*. OVX, $^{\$\$}$ $P \leq 0.01$ *vs*. OVX $CaCO_3$ (one-way ANOVA test followed by Tukey's HSD post hoc test to adjust for multiple comparisons).

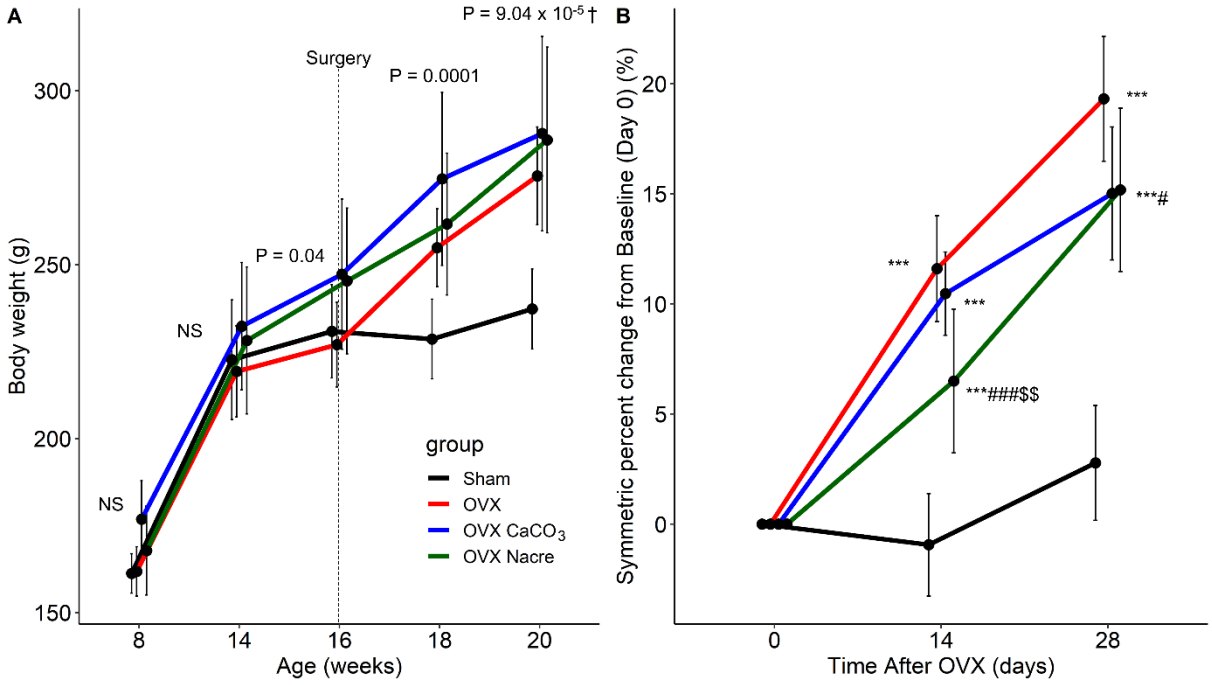

Figure S2. The morphological trabecular parameters in the proximal tibia in *ex vivo* cross-sectional study. µCT scout image in which the box depicts a scanned region of 147 consecutive slices (10.5 µm/slice) analyzed for trabecular bone volume, as detailed in Methods (**A**). Representative 3D images of the trabecular bone microarchitecture in the right proximal tibia **(B)**. Quantitative results of µCT analysis expressed as BV/TV, Conn.D, Tb.N, Tb.Th, Tb.Sp, SMI (**C-H)**. Data represent as boxplots, and show all data points, with interquartile range (IQR) (height of the box), median (internal horizontal bar) (n=10 per group), and mean marked by a black asterisk in the box. * $P \leq 0.05$, ** $P \leq 0.01$, *** $P \leq 0.001$, **** $P \leq 0.0001$; * *vs.* Sham, # *vs.* OVX, $ *vs.* OVX $CaCO_3$ (Kruskal-Wallis test followed by Mann-Whitney-Wilcoxon unpaired test with Benjamini-Hochberg adjustment).

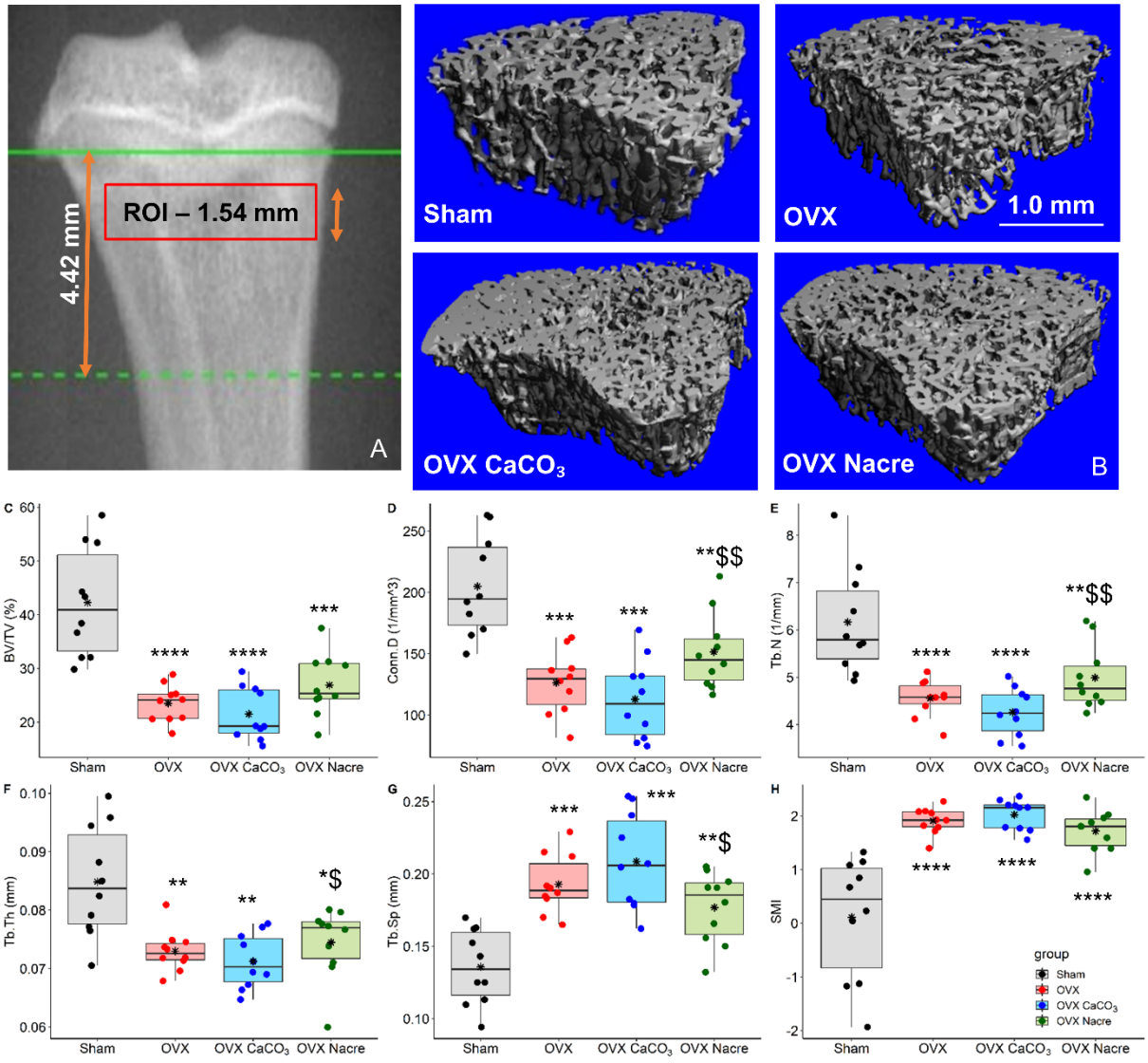

Figure S3. **Quantitative results of µCT *ex vivo* analysis in the distal metaphyseal femur expressed as BV/TV, Conn.D, Tb.N, Tb.Th and Tb.Sp, SMI**. Data represent as boxplots, and show all data points, with interquartile range (IQR) (height of the box), median (internal horizontal bar) (n=10 per group), mean (black asterisk in the box, *). * $P \leq 0.05$, ** $P \leq 0.01$, *** $P \leq 0.001$, **** $P \leq 0.0001$; * *vs.* Sham group, $^{\#}$ *vs.* OVX group, $^{\$}$ *vs.* OVX $CaCO_3$ group (Kruskal-Wallis test followed by Mann-Whitney-Wilcoxon unpaired test with Benjamini-Hochberg adjustment).

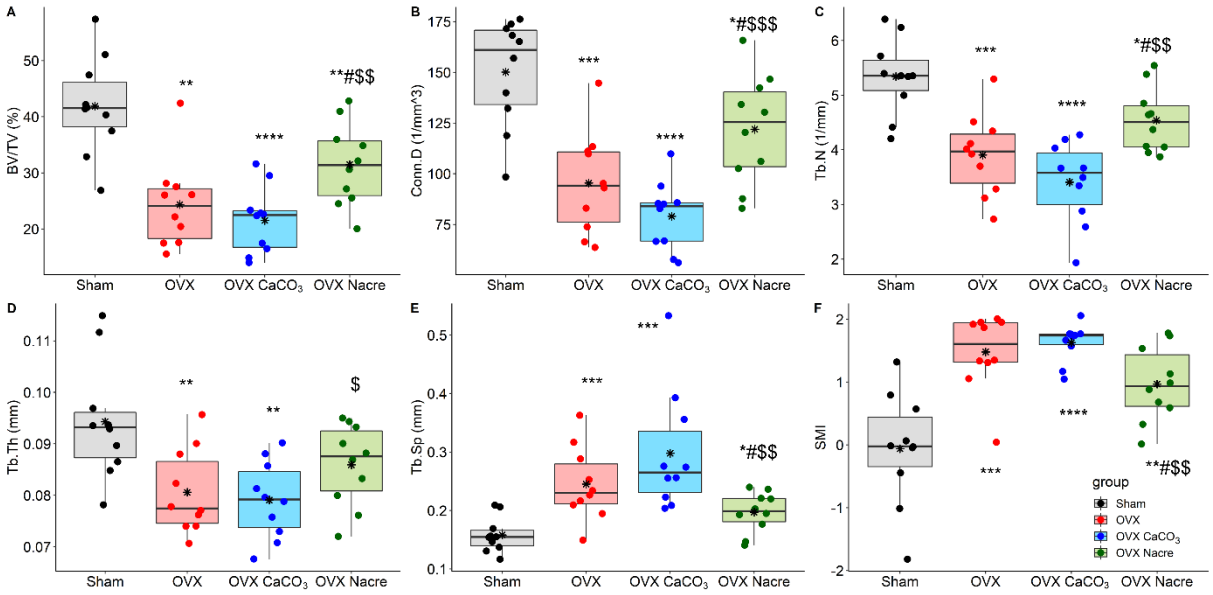

Figure S4. **Location of skeletal sites was analyzed using µCT**. µCT scout images of the appendicular bones: diaphyseal tibia in a longitudinal study (*in vivo*) **(A1),** and is a cross-sectional study (*ex vivo)* ***(*A2)**, diaphyseal femur **(A3)** show the scanned region and ROIs for cortical bone measurements. µCT scout image of the axial bone, 2nd lumbar spine (LS2) shows the scanned region and trabecular ROI for trabecular bone measurement **(B1)**, 2-dimensional coronal slice shows ROI (drawn in green) through trabecular body region **(B2)**, representative 3-dimensional images of the trabecular bone microarchitecture **(B3)**.

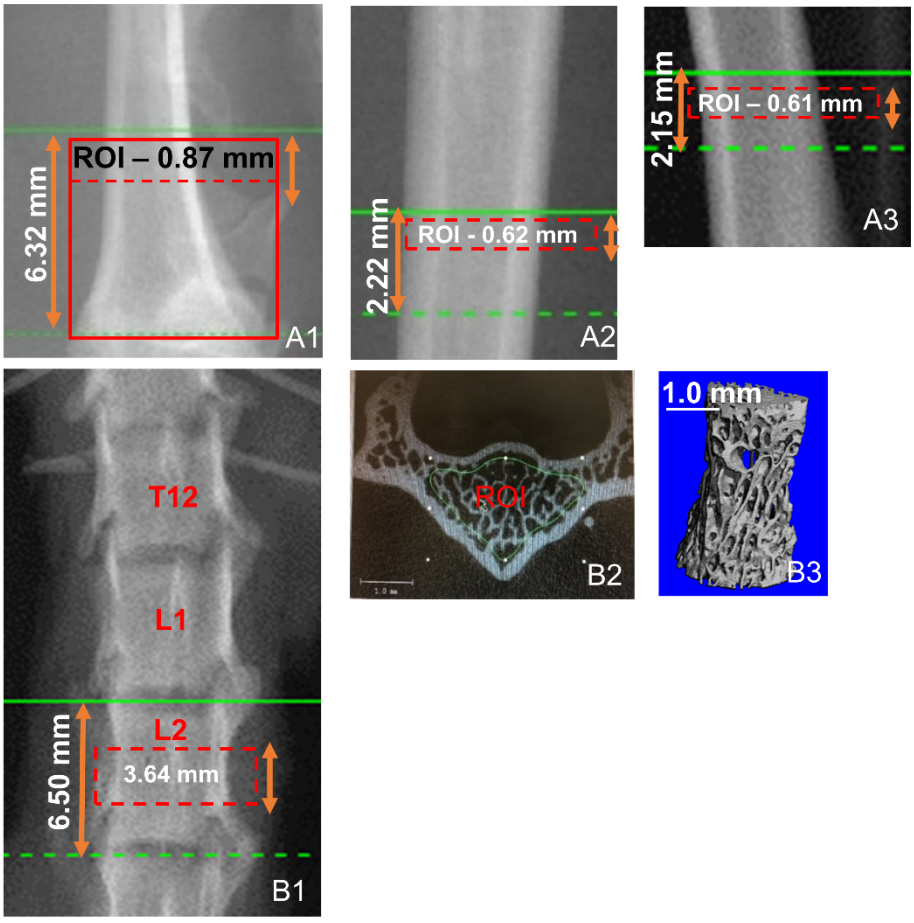

Figure S5. Changes in plasma PTH (A) and serum Calcium (B), plasma FGF23 (C), and serum Phosphate (D) from baseline to follow-ups in the OVX and OVX Nacre groups. The data were represented as the mean ± standard error (vertical bar) (n=6 per group). P-values indicated the effect of group (between-subjects factor) and/or time (within-subjects factor) and the group x time interaction using two-way repeated-measures ANOVA, followed by Tukey's HSD posthoc test to adjust for multiple comparisons. $^{\#}$ $P \leq 0.05$. $^{\#}$ *vs*. OVX, $^{\$}$ *vs*. OVX $CaCO_3$; $^{£}$ *vs*. baseline at day 0, $^{¤}$ *vs*. follow-up at day 14.

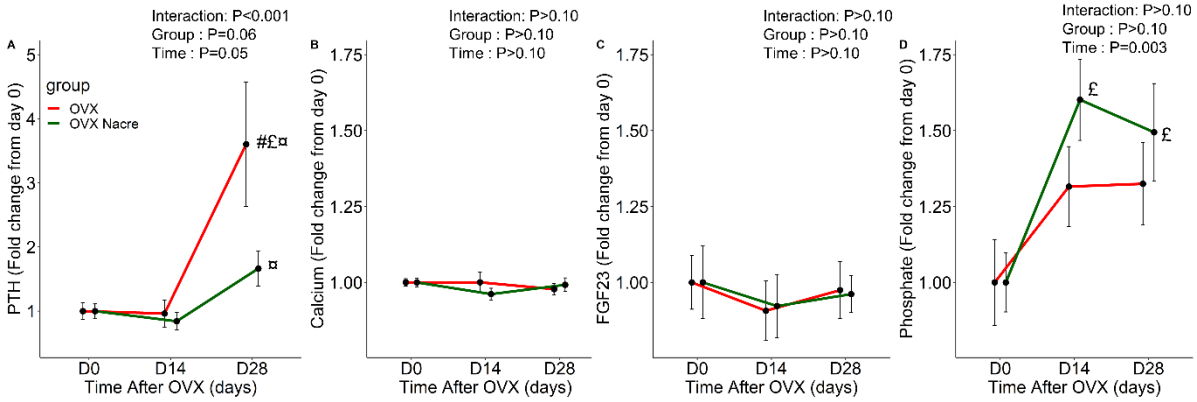

Section 5: ARRIVE guidelines Checklist B (see in file pdf)

References

1. Bouxsein ML, Boyd SK, Christiansen BA, Guldberg RE, Jepsen KJ, Müller R. Guidelines for assessment of bone microstructure in rodents using micro–computed tomography. Journal of bone and mineral research. 2010;25(7):1468-86.
2. Dempster DW, Compston JE, Drezner MK, Glorieux FH, Kanis JA, Malluche H, et al. Standardized nomenclature, symbols, and units for bone histomorphometry: a 2012 update of the report of the ASBMR Histomorphometry Nomenclature Committee. Journal of bone and mineral research: the official journal of the American Society for Bone and Mineral Research. 2013;28(1):2.
3. Bourrat X, Francke L, Lopez E, Rousseau M, Stempflé P, Angellier M, et al. Nacre biocrystal thermal behaviour. CrystEngComm. 2007;9(12):1205-8.